DESIGN AND IMPLEMENTATION OF ENERGY HARVESTING DEVICE USING VEHICLE SUSPENSION SYSTEM

by

Yi Pu

Submitted in partial fulfilment of the
requirements for the degree of
Master of Applied Science

at

Dalhousie University
Halifax, Nova Scotia
March 2015

To my Mother Baoxia Guo, and my Father Jiexin Pu

TABLE OF CONTENTS

LIST OF TABLES

LIST OF FIGURES

ABSTRACT

Vibration energy is widely distributed in people's daily life. Researching on a vibration device to transform vibration energy into electrical energy, and act as a supplementation to the power generation system, is of great significance to better developing and exploiting new energy. This thesis constructs an experiment system which consists of permanent-magnet linear generator, digital signal processor (DSP), Energy Management System. The micro controller unit (MCU) is adopted to control simulated vibration environment. The MCU control circuit and DC-DC converter circuit have been designed, and the corresponding printed circuit boards have been made. Based on the fuzzy proportional-integral (PI) control algorithm, the output voltage reaches 3.0V stably when the vibration frequency and load resistance are 10Hz and 20Ω, respectively. Experiment results have verified the practicability of our power generation system's design scheme using automobile vibration and the validity of fuzzy PI control algorithm the power management system used.

LIST OF ABBREVIATIONS AND SYMBOLS USED

MCU	Micro Controller Unit
DC	Direct Current
AC	Alternating Current
MOSFET	Metal–Oxide–Semiconductor Field-Effect Transistor
SCM	Single-Chip Microcomputer
PI	Proportional-Integral
PID	Proportional-Integral-Derivative
DSP	Digital Signal Processor
PMTLG	Permanent Magnet Tubular Linear Generator
PWM	Pulse Width Modulation
PFM	Pulse Frequency Modulation
SISO	Single-Input, Single-Output
DDAs	Differential Difference Amplifiers
NdFeB	Neodymium Iron Boron
ZR	Zero-Right
PS	Positive Small
PM	Positive Medium
PL	Positive Large
PB	Positive Big
PTB	Positive too Big
PC	Positive-Cover
RFC	Right Fuzzy Controller
LFC	Left Fuzzy Controller
ZL	Zero-Left

NS	Negative Small
NM	Negative Medium
NL	Negative Large
NB	Negative Big
NC	Negative-Cover
ADC	Analog-to-Digital Converter

T	Tesla
V	Volt
Hz	Hertz
Ω	Ohm

ACKNOWLEDGEMENTS

Foremost, I would like to express my sincere gratitude to my supervisor Prof. Jason Gu for the support of my M.A.Sc study and research, for his patience, motivation, enthusiasm, and immense knowledge. His guidance helped me in all the time of research and writing of this thesis. I could not have imagined having a better supervisor and mentor for my M.A.Sc study.

Besides my advisor, I would like to thank the rest of my thesis committee: Prof. Mohamed E El-Hawary and Prof. Williams J. Phillips, for their encouragement, insightful comments, and hard questions.

I thank my fellow labmates in Dr. Gu's group: Umar Farooq, Yang Xu, Zheng Chen, Zichen Zhang, Shijie Zhou, Mengjie Yang, Yuansheng Lu, Chaojiong Huang, for the stimulating discussions, for the laughter in the lab, and for all the fun we have had in the last years. Also I thank my friends in Halifax: Han Zhang, Mingwei Liu, Hao Cheng, Qihao Zhang, Dachuan Sun, Qiucheng Du, Kai Jiang, Ding He, Ran Yi, Qianru Hou. You all have been a very important part in my life. In particular, a heartfelt thanks goes out to my girlfriend Si Yu for all your love, support and patience when I was working on the thesis.

Last but not the least, I would like to thank my parents: Baoxia Guo and Jiexin Pu, for giving birth to me at the first place and supporting me spiritually throughout my life.

CHAPTER 1 INTRODUCTION

1.1 Introduction

The modernization of the world benefited from fossil energy, such as the widely used of the oil, natural gas, coal and other energy. These non-renewable energy not only face the exhaustion of the crisis, and a lot of use of fossil fuels destroyed the ecological environment, caused negative impact on the development of human society development. Therefore, the development of novel renewable energy, such as bioenergy, solar, wind energy, tidal energy and vibrational energy, has become the focus of attention of the society. The researchers in the world have been already focus on the renewable energy power generation technology. Among them, the solar energy, wind energy and bioenergy has already tended to be mature gradually, the vibrational energy power generation technology is still in the research stage, and is becoming a new hotspot of researchers.

Vibration energy is ubiquitous, such as the moving vehicles, the vibration of piston and the heart beats, which are all the vibration energy in our daily life. However, most of these energy are absorbed by the vibration device or wasted [1]. This thesis will focus on the study of vehicle vibration energy harvesting device and the design and development of power converter system.

1.2 The Development and Research Status

1.2.1 Permanent-Magnet Vibration Linear Generator

Linear motor is an electrical device which use the linear motion of the rotor to generate electricity or use electricity to produce linear motion. In 1840, a British named Charles Wheastone invented the first linear motor prototype in the world, but he failed due to the large air gap and led to the low efficiency. In 1845, he improved the linear motor which laid the groundwork for future research and development. Since then, the linear motor has gone through from explore, test, development and application to commercialization. The development of linear motor is rapid, some researchers and companies from developed countries have thrown lots of manpower and material on it, and they already have the high quality products [2]. But it is limited to the research and application of permanent magnet linear motor, the research of permanent magnet linear generator did not has further development until the recent decades. At present the application of permanent magnet linear generator system is mainly used on the auto feedback power generation and ocean energy absorption. For the vibration energy generation on permanent magnet linear generator research began in recent years, so there is a lack of the relevant literature.

In the wave power system, the early researchers used a rotary motor as power converters [3]. This motor has the middle conversion device, such as air cylinder, gear, that need to convert the reciprocating motion of the waves into mechanical energy, then convert into

electricity, so it has the complex structure, difficult to maintain and low efficiency shortcomings. However, the wave power system that composed of the linear motor, eliminating the middle conversion device, has the advantages such as simple structure, easy to maintain and high efficiency [4]-[6]. [7] [8] using the numerical analysis and the finite element analysis, introduces the method of optimization design of permanent magnet tubular linear generator (PMTLG). [9] used a slot-less cylinder permanent magnet linear generator to harvest the wave energy, but the generator power density and the conversion efficiency are low. The permanent magnet linear motor using Halbach magnetization [10], although the air gap flux density is close to sine, it is difficult to machining and the cost is high. [11] [12] proposed a large Archimides made of wave power system using permanent magnet linear motor, but the system is essential to the waters of choice, high cost, and long construction period and installation issues. Oregon state university and the United States navy developed a point of suction wave power system [13] [14], the system is composed of cylinder permanent magnet linear motor and float, and put into use in 2012. The magnetization of permanent magnet linear motor in the system is the radial direction, and the air gap magnetic flux density is relatively low. Uppsala University [15] [16] developed a power generation system which put the linear motor at the bottom of the sea (the linear motor is made up by four flat motor), and the float through the flexible connection point suction. The system once the installation dimensions vary slightly, it will cause a lot of normal force. [17] design and manufacture a set of direct-drive type wave power system, the system adopts the cylinder type linear generator, the permanent magnet (dynamic) in

the outside, using Quasi-Halbach magnetization, compared with the structure of radial magnetization, Quasi-Halbach magnetization can improve the density of air gap and the sine degree, improve the power density of permanent magnet linear motor. [18] in order to improve efficiency of the small ocean surface wave energy converted into electrical energy, this paper proposes a cylinder type structure model of single-phase linear Halbach permanent magnet generator, finite element analysis of the single-phase linear permanent magnet generator internal electromagnetic field dynamic characteristics were analyzed, and optimized the motor tooth structure. Cylinder type single-phase linear Halbach permanent magnet generator has high sinusoidal magnetic field, small positioning force fluctuation amplitude and high energy conversion efficiency, also it is simple structure, low application cost.

In the vibration power systems field, with the widely use of various kinds of electronic equipment, power supply system has become a prominent problem that restrict the development of these devices, especially for some is unable to provide power supply, need to work a long time or the batteries are not easy to replace or in inflammable and explosive place, it need to use passive mode power supply. Therefore, from power supply technology has been rapid development in recent years [19], there have been a variety of different forms of self-energized technology, and this technology is mainly to transfer mechanical energy into electrical energy. However, due to the restriction of various conditions, self-energized technology only provides low energy, except for some specific application. The

electric power from power supply technology is not enough to meet the needs of most electronic devices at present. How to make use of more widely existing mechanical energy converting it into electricity, and how to improve the conversion efficiency of self-energized technology is a problem that needs to be solved in passive electronic technology field.

1.2.2 DC-DC Converter

DC-DC converter is to convert the uncontrollable DC voltage into another controllable DC voltage, to meet the requirements of electronic equipment, has been widely applied in all kinds of instruments and meters. There are three types of DC-DC converter: DC-DC Buck converter, DC-DC Boost converter and DC-DC Buck-Boost converter. There are three control mode for DC-DC converter: Pulse Width Modulation (PWM) mode, Pulse Frequency Modulation (PFM) mode and PWM/PFM conversion mode. PWM mode has high efficiency and good output voltage ripple and noise; PFM mode has small power consumption for small load. In PWM/PFM conversion mode, PFM is working when using small load, PWM is working when using heavy load. Now, The DC-DC converter is widely used in mobile phone, MP3, digital cameras, portable media players and other products.

In recent years, in order to improve the performance and control issues of the DC - DC converter, many researchers have carried out extensive and in-depth study. [20] was studied by sampling output feedback control problem of uncertain data, designed a robust output

feedback controller and the reduced order observer, developed a DC-DC voltage power supply converter, mixed closed-loop DC-DC output voltage of the Buck converter system will globally asymptotically tends to set data, the method is direct and simple. [21] proposed a resonant switching multistage dc boost converter, also known as the multiplier of the boost converter, its peak type electric current in the capacitor is eliminated by a resonant inductance, implements the resonant current waveform. [22] studied the robust control problem of output voltage regulator of the boost converter. Its control method is to use time delay switch input to the inverter, and the output current and voltage variables, instead of unknown dynamic and interference, control the output voltage of capacitor to keep with fast response under the input voltage change of output voltage constant and decrease overshoot, improves the load changes because of the connection state variables and system parameter changes the system input dry winding resistance. [23] designed a self-tuning fuzzy proportional-integral-derivative (PID) controller of PWM DC-DC converter, which combined fuzzy control with conventional PID controller, the self-tuning fuzzy PID controller could adjust their parameters to achieve better performance of control system. [24] proposed a new boost converter using the differential difference amplifiers (DDAs) in the control loop. Compared with the traditional current mode boost converter, the circuit of the controller is simpler and less power consumption. [25] presents a resonant DC-DC converter suitable for ultra-low power and low voltage sources. The input low voltage is stepped-up to a conventional level of some volts, what allows to power autonomously and solely low power circuits from energy harvesting sources. [26] presents

an original self-starting DC/DC converter for low-power and low-voltage applications such as energy harvesting from m icrobial fuel cells to supply low-power electronic devices. The harvested power reaches 10 mW under 0.3 V input voltage for the ten 1.3-liter experimental microbial fuel cells connected in parallel. [27] proposes a high-efficiency dc-dc converter with fast dynamic response for low-voltage photovoltaic sources.

1.3 Thesis Objectives

Vehicle vibration energy can be collected from the general suspension system with energy conversion device, with the space constraints, the electromechanical conversion device cannot be too large. There is quite lack of the literature in the permanent magnet linear generator field. In the thesis, the permanent magnet linear generator is chosen as the vehicle vibration energy harvesting device. Therefore, the first objective is the design of the permanent magnet linear generator.

In order to make the vehicle vibration energy harvesting device better used in automotive electronic devices, how to transfer the generator output to the effective output voltage is very important. Hence, the DC-DC converter is another objective of this thesis.

1.4 Thesis Organization

Chapter 1 Introduces vehicle vibration energy harvesting system, reviews recent advance of permanent magnet vibration linear generator, DC-DC converter, and states the objective

of this thesis. Chapter 2 Introduces the structure and rationale of linear generator. A slot less design of permanent magnet linear generator is presented, simulated and tested in this chapter. Chapter 3 analyses and models the DC-DC converter. Proposes the customized DC-DC converter for the vehicle vibration energy harvesting system. Chapter 4, in this chapter, a new model for a single-input, single output (SISO) control method is presented. This model is obtained by switching fuzzy proportional-integral controller designed for output voltage regulation. Simulation results verify the model. Chapter 5 presents the three parts of the experiment system. Laboratory test the vehicle vibration energy harvesting system and results are reported. Chapter 6 summarizes the contributions in the thesis and suggests future work.

CHAPTER 2 DESIGN OF PERMANENT-MAGNET VIBRATION LINEAR GENERATOR

2.1 Introduction

Most linear generator can be thought of as a rotary generator in the structure of a kind of evolution, it can be seen as a rotary generator along the radial cut open, and the circumference of the generator show in a straight line. The theory and structure are same with the rotary generator.

In this thesis, the proposed linear generator has the different structure with the classical linear generator.

2.1.1 Structure of Linear Generator

Figure 2-1 shows stator core axis section of the rotary generator. The stator is a cylinder with multiple circular grooves, which used to hold the stator windings.

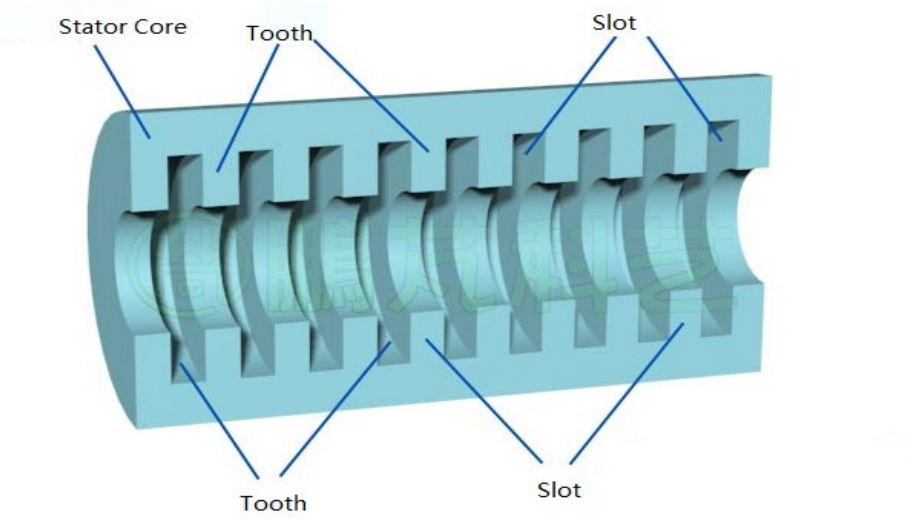

Fig. 2-1 Stator core axis section

In a linear generator the moving part is the rotor which is “unrolled” and consists of magnetic yoke and permanent magnets. The magnetic yoke is magnetizer and the magnetic pathways between magnetic poles. The permanent magnets are in the magnetic peripheral. Figure 2-2 is the rotor of a linear generator.

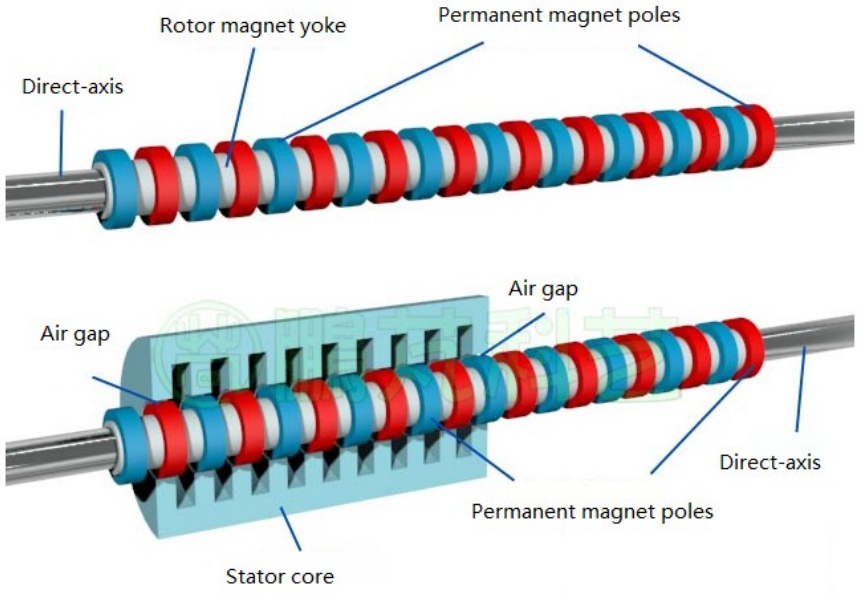

Fig. 2-2 Rotor of the linear generator

2.1.2 Rationale of Linear Generator

Figure 2-3 is the linear generator in section. The dynamic magnetic pole of permanent magnet flux direction is perpendicular to the axis of the linear generator.

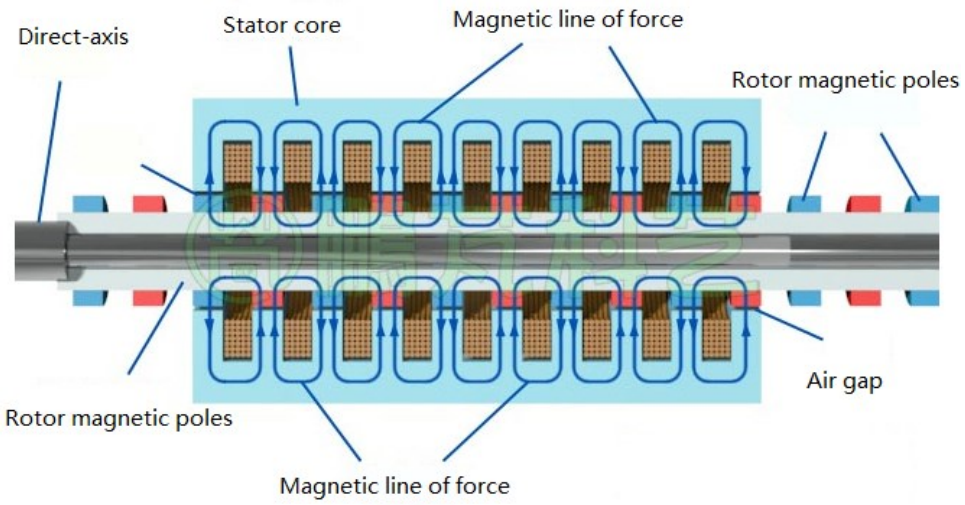

Fig. 2-3 Magnetic flux direction of the linear generator

If all blue magnetic flux is deviate from the axis direction, then all red magnetic flux direction is toward the axis, we can get the magnetic field lines path diagram in Figure 2-3. The magnetic field lines are outwards from the blue magnetic pole through the air gap into the stator core, and bypass the windings in the stator core through the air gap to the red magnetic pole, after rotor magnetic yoke back to blue magnetic pole, form a loop.

When the rotor moves a slot to left, the magnetic field lines are still outwards from the blue magnetic pole through the air gap, bypass the windings in the stator core through the air gap to the red magnetic pole. But the magnetic flux direction around each coil contrary to the Figure 2-4. When the rotor has a continuous movement, the magnetic flux direction

through the coil will turnover, and the coil will induce the alternating current (AC) electric potential.

The direction of adjacent coil inducted electric potential is opposite. Connect all the coils according to the polarity. It is a single phase AC linear generator

2.2 Design of Permanent-Magnet Vibration Linear Generator

2.2.1 Body Design

There were two possible linear generator designs which was proposed for the project. They were:

a. Slot Less Design

- Uses windings with a ferrous backing. In this case it would be a steel tube with cylindrical windings inside it and the shaft with the magnets on it inside that.

- Does not have cogging force because distance between the magnets and the ferrous material is uniform along the length of the shaft.

- Very simple to construct. This is because windings can be wound on the outside of a

cylindrical piece of plastic and slide inside the steel tube. Not much machining would need to be done.

- Since there is no ferrous material between the windings the air gap in the generator is the width of the windings. Having such a large air gap in the magnet circuit means that flux densities in this design can be improved.

- This design was already used by another research team.

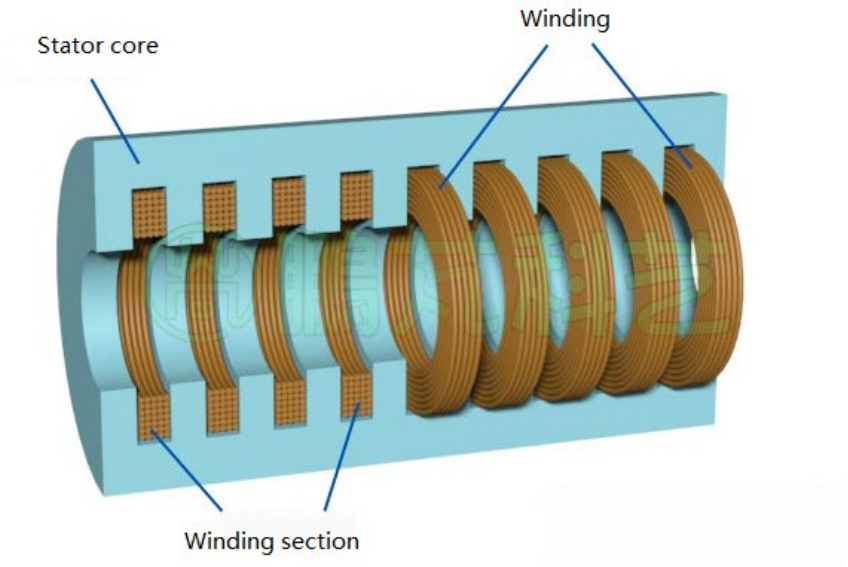

Fig. 2-4 Stator cores and winding of the slotted design

b. Slotted Design

- Windings are held in slots on the inside of a cylindrical steel tube. The magnets are located on the shaft.

- This design is affected by cogging due to the slots in the steel. However this can be reduced by in two ways:

    - Skewing the magnets. This is the method normally used in rotary motors. However in this case the magnets need to fit around a shaft and reducing cogging this way would require custom made magnets and increase costs significantly.

    - Skewing the windings. Implementing this method with produce the same effect as skewing the magnets. This can be done by machining the winding separators so that they sit in the tube at an angle. This is done so that the poles line up with different slots on either side of the tube.

- Due to the requirement of slots on the inside of a cylindrical tube for this design, machining could be more difficult than with a slot less design.

- A slotted design provides the best possible energy densities and is superior to the slot less design in that regard. Flux densities are reduced somewhat by skewing of the windings but it is still the most efficient generator.

The cross-section drawn of the proposed permanent-magnet linear generator shows in Fig.

2-4.

The Slotted Linear generator design was selected due to its increased flux densities over other designs. In order to reduce cogging skewed windings would the ideal method to use, however fabrication would be difficult, therefore skewed windings were not used. A bushing was pressed into the end cap to maintain the linearity of the shaft with a wiper seal likely to be used to seal off the generator from the outside.

2.2.2 Material Selection

Rare-earth permanent magnet has the high remanence, high coercive force, high magnetic energy product, and linear demagnetization curve. So the rare-earth permanent generator is high efficiency, high quality, lightweight and more reliable. The permanent magnet generator has widespread development due to the rapid development of the rare-earth permanent magnet. Permanent magnet generator overcome the long drive chain, low efficiency and poor accuracy that exist in the transmission mechanism of the traditional rotating generator, and is favored by more and more researchers with the simple structure, high efficiency and low power consumption.

Permanent magnet is one of the core components of the permanent magnet linear generator, and the quality of the permanent magnet material directly affects the performance of the generator. It has many different permanent magnet materials, such as Alnico magnet,

Ferrite magnet, Rare-earth samarium cobalt magnet and Neodymium iron boron (NdFeB) magnet.

There are two kinds of Alnico magnet, cast molding and powder. They both have high magnetic remanence, good high thermal stability but low coercive force. Also, the cast molding Alnico magnet is hard to machining, and the powder Alnico magnet is very expensive. Ferrite magnet has high coercive force, but low magnetic remanence, high temperature coefficient, is not applicable in the wide temperature differential environment. Rare-earth samarium cobalt magnet has high coercive force, good magnetism stability, allow working temperature up to 200~250 degree centigrade, but very high cost. $Nd_2Fe_{14}B$ is the major components of NdFeB magnet, and one of the strongest magnetic materials. Its maximum magnetic energy product could reach 398 kJ/m^3, the remanence is up to 1.47 T, the coercive force could be over 1000 kA/m. Also, it has high mechanical strength and low cost.

The performance and characteristics of commonly used permanent magnet materials as shown in table 2-1.

Table 2-1 The properties and characteristics of common permanent magnet material

	Permanent magnet material				
	AlNiCo	Ba-Ferrite	SmCo(1:5)	SmCo(2:17)	NdFeB

Remanence Br/(T)	0.8-1.4	0.2-0.44	0.85-1.05	1-1.14	1.1-1.52
Coercive force Hc/(kA/m)	38-155	143-318	637-796	717-844	796-1115
Intrinsic coercive force Hcj/(kA/m)	40-159	159-358	1194-2388	1194-2388	955-2388
Maximum magnetic energy product (BH)max/(kJ/m^3)	8-88	8-36	127-207	175-255	239-446
Temperature coefficient of remanence a/(%/℃)	-(0.02-0.03)	-(0.18-0.19)	-(0.04-0.05)	-0.03	-0.01
Intrinsic coercive force temperature coefficient β/（%/℃）	N/A	0.20-0.60	-(0.30-0.35)	-(0.03-0.05)	-(0.45-0.6)
Recoil permeability μ_{rec}	1.3-5.2	1.05-1.10	1.02-1.10	1.05-1.10	1.05-1.10
Curie point T_c/(℃)	800-860	465	750	800-850	312-420

The remanence and maximum magnetic energy product are two of important performance index of permanent magnet materials. In practical application, the bigger magnetic field intensity of the permanent magnet in the air gap is better. The maximum magnetic field intensity in the air gap depends on the remanence and maximum magnetic energy product

of the materials. Therefore, it needs the bigger remanence and maximum magnetic energy product of the materials to improve the magnetic field intensity of the permanent magnet in the air gap. On the side, for some certain air gap and air gap magnetic field, the more magnetic energy product of the materials it has, the less materials it needs and the lower it costs.

NdFeB magnet is chosen for this permanent magnet generator. The magnetic parameters are shown in table 2-2.

Table 2-2 Magnetic parameters of NdFeB magnet

Remanence Br	Coercive force Hc	Intrinsic coercive force Hcj	Maximum magnetic energy product (BH)max	Density	Recoil permeability	Operating temperature Tw
T	kA/m	kA/m	kJ/m^3	g/cm^3	μ	℃
1.22-.125	899-907	>955	287-310	7.5	1.05	80

2.3 Simulation and Test of the Permanent-Magnet Vibration Linear Generator

The linear generator design that was selected uses is slotted and has the windings sitting in

slots on the inside of the cylinder. The moving part has a stack of axially polarized magnets where each magnet is separated by a steel spacer to provide a flux path, without the spacer the flux would not enter the windings.

Figure 2-5 shows the flux density plot of the generator. In this position the maximum amount of flux is in the windings. The average flux density in the windings was about 0.2T at its peak. This drops to close to 0T at its minimum.

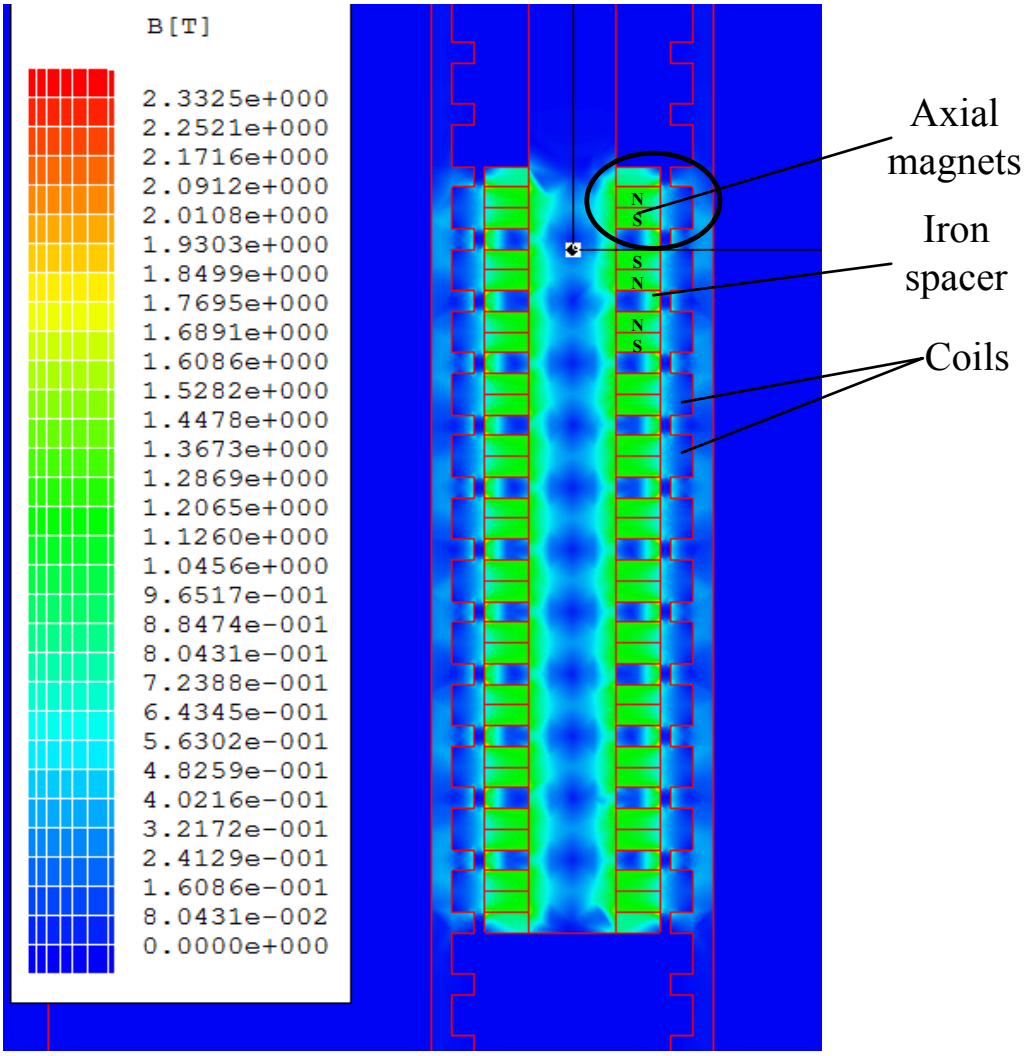

Fig. 2-5 Diagram of magnetic flux density

In this design the field is completely cycled with 0.25 inches of movement. This gives an oscillating output wave form with a period that corresponds to the time that it took to move the forcer 0.25 inches. By measuring the period the velocity of the forcer can be calculated. This is useful because any large movement where dampening should be controlled will have a movement much greater than 0.25 inches and since damping is a velocity dependent force the velocity is what needs to be measured.

Table 2-3 Properties list

Number of Windings	20
Number of Turns Per Winding	100
Area of Windings	6.41 cm^2
Number of Windings Excited	10
B_{max}	0.2T

Using faraday's law and the parameters from table 2-3, an excel spread sheet model for the operation of the generator was developed. The excel spreadsheet took into account the number of turns per winding, the number of windings excited at any time and the maximum flux density of the This gives the output voltage in relation the velocity of the forcer. Figure 6 shows a plot of this relationship the motor constant is the slope of this line which is k=18.2 Vs/m.

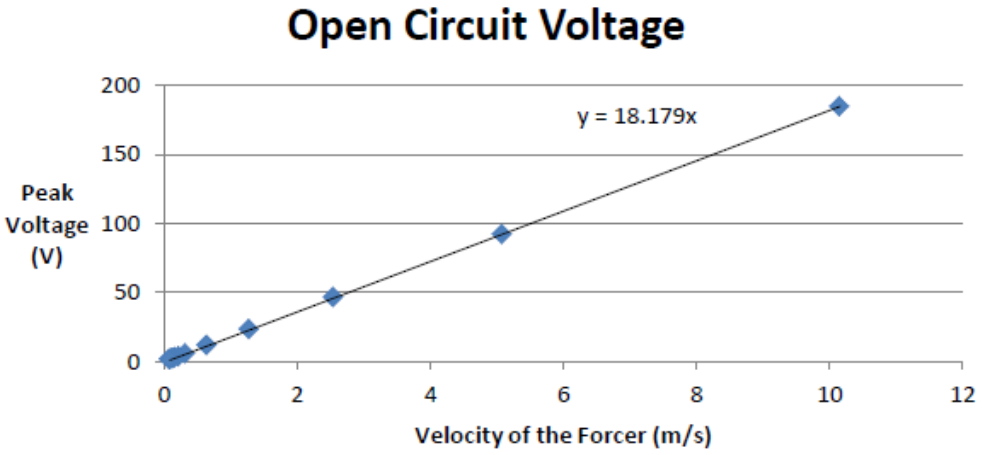

Fig. 2-6 Output voltage in relation to the velocity of the forcer

The output shown in figure 2-7 is what was expected for the output waveform of the generator. This shows the forcer being moved by hand, as the forcer is moved by ¼ inch a full period of oscillation occurs. This is why there is a higher frequency component in the waveform. The output waveform is exactly what it was expected to be from the modeling done in the design. By measuring the period of the higher frequency oscillation the velocity could be determined. From these velocity measurements the actual motor constant for the device was determined to be about 16Vs/m. This is slightly less than what was expected from the model, but the difference is small enough that it can be attributed to the generator not being entirely functional yet due to the high friction.

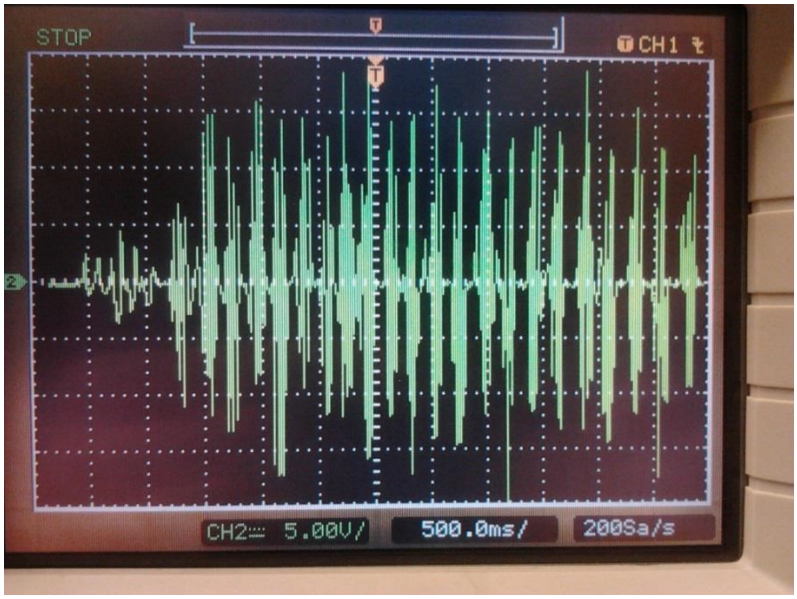

Fig. 2-7 Test results

From figure 2-8 the maximum velocity reached was 1.6m/s and the output voltage was 19V.

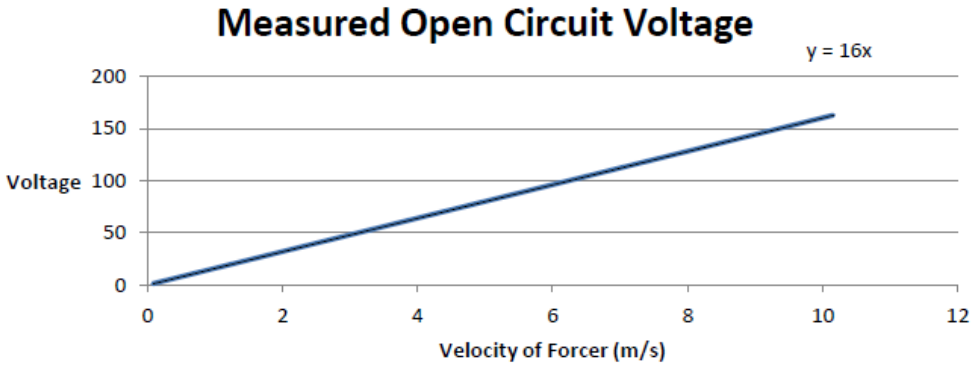

Fig. 2-8 Measured open circuit voltage

2.4 Summary

In this section, analysis of the data clearly indicates the viability of the body design of the linear generator. The modeling the slotted design clearly showed the improvements in

electrical and magnetic properties over the normal design, and the results from the test was able to perform shows expected results. However the generator design that was chosen was significantly more complicated due to the number of windings involved and fabrication was very difficult.

CHAPTER 3 DESIGN, ANALYSIS AND DEVELOPMENT OF DC-DC CONVERTER

3.1 Rationale of Buck-Boost

3.1.1 Main Circuit Topology and Working Principle

The Buck-Boost converter is a type of DC-DC converter that has an output voltage magnitude which is either larger than or less than the input voltage magnitude. The main circuit consists of switching tube, diodes, inductors, capacitors. The polarity of the output voltage of the circuit and the input voltage are opposite. Buck-Boost converter has continuous current mode and discontinuous current mode [28].

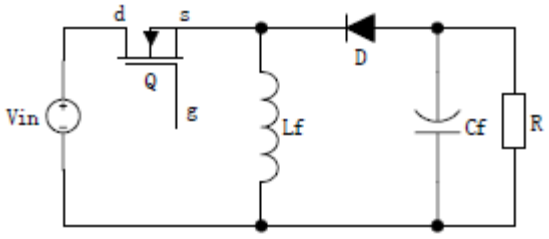

Fig. 3-1 Buck-Boost main circuit

3.1.2 Rationale and Relation Formula of the Buck-Boost Converter Continuous Current Mode

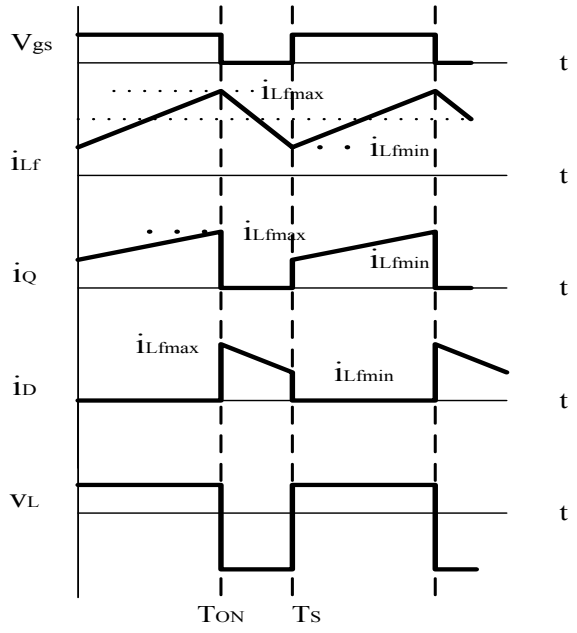

Fig. 3-2 Continuous current mode

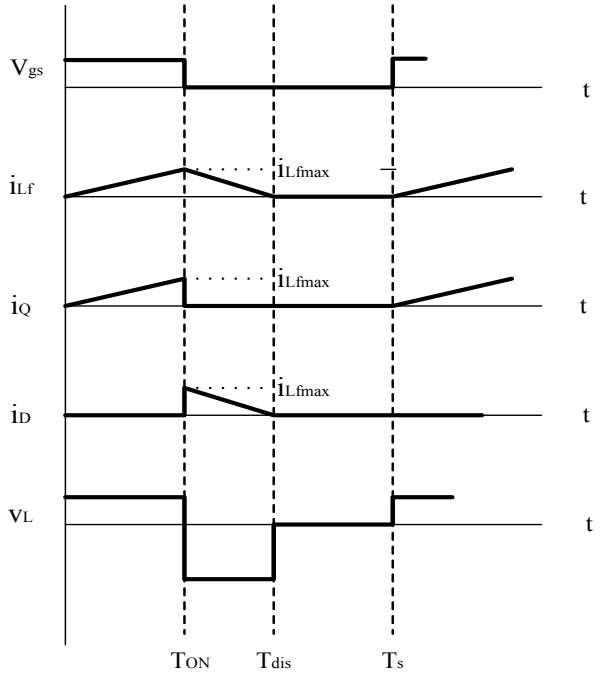

Fig. 3-3 Discontinuous current mode

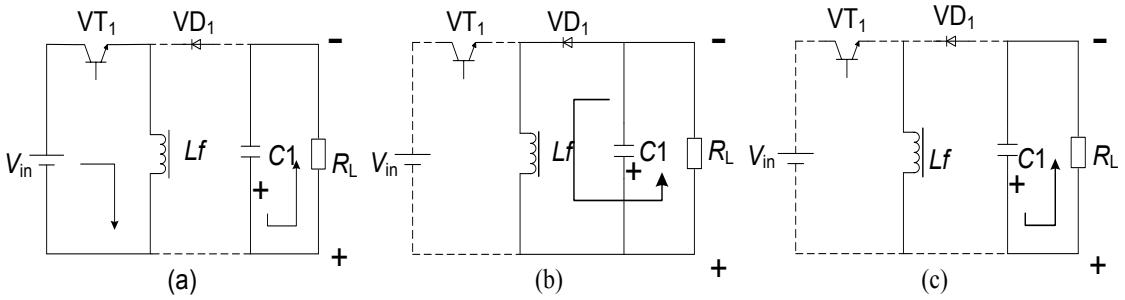

Fig. 3-4 Three switch modes equivalent circuits of Buck-Boost converter

(a) VT_1 is on; (b) VT_1 is off; (c) Inductor current is 0 when VT_1 is off

3.1.2.1 Rationale of the continuous current mode

1) Switching mode 1 [0, T_{ON}] (Fig. 3-4(a))

When t=0, switch Q is on, the power supply voltage V_{in} is all on the inductor L, the inductor current i_{Lf} increases linearly, the diode D is cut off, the load is powered by the filter capacitor C.

$$L_f \frac{\mathrm{d}i_{Lf}}{\mathrm{d}t} = V_{in} \tag{3.1}$$

When t=T_{on}, i_{Lf} reaches the maximum i_{Lfmax}. During the switch Q is on, the increase of $i_{Lf(+)}$ is:

$$\Delta i_{Lf(+)} = \frac{V_{in}}{L_f} T_{ON} = \frac{V_{in}}{L_f} D_y T_s \tag{3.2}$$

2) Switching mode 2 [T_{ON}, T_s] (Fig. 3-4(b))

When t=T_{ON}, the switch Q is off, i_{Lf} has continued flow through the diode D, the power of L_f transfers to load and capacitor C_f. At this point, the voltage of L_f is – V_0, i_{Lf} decreases linearly.

$$L_f \frac{\mathrm{d}i_{Lf}}{\mathrm{dt}} = -V_0 \tag{3.3}$$

When $t=T_s$, i_{Lf} reaches the minimum i_{Lfmin}. During the switch Q is off, the decrease of $i_{Lf(-)}$ is:

$$\Delta i_{Lf(-)} = \frac{V_0}{L_f}(T_s - T_{ON}) = \frac{V_0}{L_f}(1 - D_y)T_s \tag{3.4}$$

3.1.2.2 Relation formula of the continuous current mode

When working in the steady state, the increase of inductive current $\Delta i_{Lf(+)}$ equals to the decrease of inductive current $\Delta i_{Lf(-)}$ during the switch Q is off. From the equation (3.2) and (3.4),

$$\frac{V_0}{V_{in}} = \frac{D_y}{1 - D_y} \tag{3.5}$$

If ignore the loss,

$$\frac{I_0}{I_{in}} = \frac{1 - D_y}{D_y} \tag{3.6}$$

When switch Q is off, the voltage of the switch V_Q is:

$$V_Q = V_{in} + V_0 = \frac{V_{in}}{1 - D_y} = \frac{V_0}{D_y} \tag{3.7}$$

When switch Q is off, the voltage of the diode V_D is:

$$V_D = V_{in} + V_0 = \frac{V_{in}}{1 - D_y} = \frac{V_0}{D_y} \tag{3.8}$$

The mean of inductive current I_{Lf} is:

$$I_{Lf} = \frac{I_{in}}{D_y} = \frac{I_0}{1 - D_y} \tag{3.9}$$

The mean of the current through the switch Q is the input-current I_{Lf}, where the

effective value is:

$$I_{Qrms} = \sqrt{\frac{1}{T_s}\int_0^{T_s} i_Q^2\, dt} = I_{Lf}\sqrt{D_y(1+\frac{\Delta i_{Lf}^2}{3I_{Lf}^2})} \tag{3.10}$$

The mean of the current through the diode D is the output-current I_o, where the effective value is :

$$I_{Drms} = \sqrt{\frac{1}{T_s}\int_0^{T_s} i_D^2\, dt} = I_{Lf}\sqrt{(1-D_y)(1+\frac{\Delta i_{Lf}^2}{3I_{Lf}^2})} \tag{3.11}$$

The mean of current through the inductor L_f is I_{Lf}, where the effective value is:

$$I_{Lrms} = \sqrt{\frac{1}{T_s}\int_0^{T_s} i_{Lf}^2\, dt} = I_{Lf}\sqrt{1+\frac{\Delta i_{Lf}^2}{3I_{Lf}^2}} \tag{3.12}$$

The maximum current of switch Q and diode D is:

$$I_{Qmax} = I_{Dmax} = I_{Lfmax} = \frac{I_O}{1-D_y} + \frac{V_o}{2L_f f_s}\left(1-D_y\right) \tag{3.13}$$

The output voltage ripple ΔV_o is:

$$\Delta V_o = \frac{D_y}{C_f f_s} I_o \tag{3.14}$$

3.1.3 Rationale and Relation Formula of the Buck-Boost Converter Discontinuous Current Mode

3.1.3.1 Rationale of the discontinuous current mode

1) Switching mode 1 [0, T_{on}] (Fig. 3-4(a))

When t=0, switch Q is on, the power supply voltage V_{in} is all on the inductor L, the inductor current i_{Lf} increases linearly, the diode D is cut off, the load is powered

by the filter capacitor C.

$$L_f \frac{\mathrm{d}i_{Lf}}{\mathrm{dt}} = V_{in} \tag{3.15}$$

When t=T_{on}, i_{Lf} reaches the maximum i_{Lfmax}. During the switch Q is on, the increase of $i_{Lf(+)}$ is:

$$\Delta i_{Lf(+)} = \frac{V_{in}}{L_f} T_{ON} = \frac{V_{in}}{L_f} D_y T_s \tag{3.16}$$

2) Switching mode 2 [T_{on}, T_{dis}] (Fig. 3-4(b))

When t=T_{ON}, the switch Q is off, i_{Lf} has continued flow through the diode D, the power of L_f transfers to load and capacitor C_f. At this point, the voltage of L_f is $-V_0$, i_{Lf} decreases linearly.

$$L_f \frac{\mathrm{d}i_{Lf}}{\mathrm{dt}} = -V_0 \tag{3.17}$$

When t=T_{dis}, i_{Lf} reaches 0, the decrease of i_{Lf} is:

$$\Delta i_{Lf(-)} = \frac{V_0}{L_f}(T_{dis} - T_{ON}) = \frac{V_0}{L_f} \Delta D_y T_s \tag{3.18}$$

$$where\ \Delta D_y = \frac{T_{dis} - T_{ON}}{T_s} \tag{3.19}$$

3) Switching mode 3 [T_{ON}, T_{dis}] (Fig. 3-4(c))

In this meantime, the switch Q and diode D are both cut-off, i_{Lf} is 0, the load is powered by filter capacitor.

3.1.3.2 Relation formula of the discontinuous current mode

When working in the steady state, the increase of inductive current $\Delta i_{Lf(+)}$ equals to the decrease of inductive current $\Delta i_{Lf(-)}$ during the switch Q is on. From the equation (3.16) and

(3.18),

$$\frac{V_0}{V_{in}} = \frac{D_y}{\Delta D_y} \tag{3.20}$$

If ignore the loss,

$$\frac{I_0}{I_{in}} = \frac{\Delta D_y}{D_y} \tag{3.21}$$

The output-current of the converter I_o is:

$$I_o = \frac{1}{2} I_{Lfmax} \Delta D_y = \frac{V_{in}^2 D_y^2}{2 L_f f_s V_o} \tag{3.22}$$

The maximum current of switch Q and diode D is:

$$I_{Qmax} = I_{Dmax} = I_{Lfmax} = \frac{V_{in} D_y}{L_f f_s} = \sqrt{\frac{2 V_o I_o}{L_f f_s}} = \sqrt{\frac{2 P_o}{L_{sf} f_s}} \tag{3.23}$$

This equation indicates that the maximum current of power devices in discontinuous current mode is only determined by the output power.

3.2 Main circuit parameters design

Circuit design requirements: input DC voltage V_{in} = 0-30V, output DC voltage V_o =12V, output power P_o = 12W.

1) Inductance calculation

Based on One-third of inductor current is consecutive, design inductance L_f.

Output power P_o = 12W, input DC voltage V_{in} = 0-40V, output DC voltage V_o =12V,

switching period T_s = 250 μS.

From equation (2.5) : $D_y = V_o/(V_{in}+V_o) \approx 0.23 - 1$

Output current $I_o = P_o/V_o = 1A$

Use $I_{oG} = I_o/2 = 0.5A$

From (2.9) and (2.4) : $I_{oG} = I_{Lf}(1-D_y) = V_o(1-D_y)^2T/2L_f$

When $D_y = 0.5$, $L_f = V_o(1-D_y)^2T_s/2I_{oG} = 750\mu H$

2) Output capacitance design

From (2.14), if $\Delta V = 0.01V_o$

$C_f = D_yI_o/\Delta V_o f_s = 0.5*10*12/(0.01*12) = 1041.67\mu F$

In practical circuit, we use a 0.1μF and a 4700μF capacitance in parallel. In switching power supply with two capacitors in parallel, the larger one is to filter, the smaller one is used to eliminate the inductive characters that the larger capacitance made when it is in high frequency.

3.3 The averaging model of non-ideal Buck-Boost converter for continuous mode

The input voltage $v_{in} = V_{in} + \hat{v}_{in}$, the output voltage $v_o = V_o + \hat{v}_o$, the inductor current $i_L = I_L + \hat{\imath}_L$, the duty ration $d_y = D_y + \hat{d}_y$ [29], then:

$$d_y i_L = \left(D_y + \hat{d}_y\right)(I_L + \hat{\imath}_L) = D_y I_L + I_L \hat{d}_y + D\hat{\imath}_L + \hat{d}_y \hat{\imath}_L \quad (3.24)$$

$$d_y v_{in} = \left(D_y + \hat{d}_y\right)\left(V_{in} + \hat{v}_{in}\right)$$

$$= D_y I_{in} + V_{in}\hat{d}_y + D_y\hat{v}_{in} + \hat{d}_y\hat{v}_{in} \tag{3.25}$$

If ignore the infinitesimal of higher order,

$$d_y i_L = \left(D_y + \hat{d}_y\right)\left(I_L + \hat{\imath}_L\right) = D_y I_L + I_L\hat{d}_y + D\hat{\imath}_L \tag{3.26}$$

$$d_y v_{in} = \left(D_y + \hat{d}_y\right)\left(V_{in} + \hat{v}_{in}\right) = D_y I_{in} + V_{in}\hat{d}_y + D_y\hat{v}_{in} \tag{3.27}$$

3.3.1 Large-signal Averaging Model

Assuming that,

a) There is no stray capacitance in the power metal–oxide–semiconductor field-effect transistor (MOSFET), the on-resistance R_{ON} and off-resistance are infinite;

b) Forward resistance of the diode is R_F, forward voltage drop is V_F, off-resistance is infinite;

c) Passive components are all linear, time-invariant;

d) The components of output impedance of input voltage to AC and DC are 0.

Fig. 3-5 and Fig. 3-6 are the non-ideal PWM switch equivalent circuit diagrams that get from Fig. 3-1.

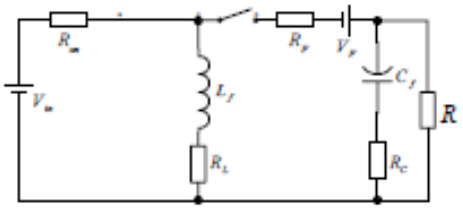

Fig. 3-5 Equivalent circuit diagram when $0 \le t \le D_y T_s$

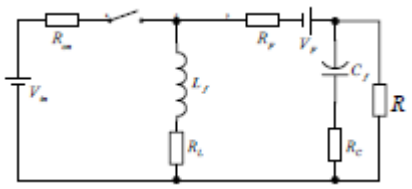

Fig. 3-6 Equivalent circuit diagram when $D_yT_s \leq t \leq T_s$

When $0 \leq t \leq D_yT_s$, S is on, D is off,

$$L_f \frac{\Delta i_{Lf(+)}}{D_yT_s} = V_{in} - I_{Lf}(R_{on} + R_L) \tag{3.28}$$

When $D_yT_s \leq t \leq T_s$, S is off, D is on,

$$L_f \frac{\Delta i_{Lf(-)}}{(1-D_{y)}T_s} = I_{Lf}(R_F + R_L) + V_F + V_o \tag{3.29}$$

The power loss of on resistances of switch Q and diode D and the loss from forward voltage drop V_F of diode D are:

$$\begin{cases} P_{Ron} = R_{on}I_{Qrms}^2 = D_yR_{on}\left(1+\dfrac{\Delta i_{Lf}^2}{3I_{Lf}^2}\right)I_{Lf}^2 = \dfrac{R_{on}}{D_y}\left(1+\dfrac{\Delta i_{Lf}^2}{3I_{Lf}^2}\right)I_{in}^2 \\ P_{RF} = R_FI_{Drms}^2 = \left(1-D_y\right)R_F\left(1+\dfrac{\Delta i_{Lf}^2}{3I_{Lf}^2}\right)I_{Lf}^2 = \dfrac{R_F}{1-D_y}\left(1+\dfrac{\Delta i_{Lf}^2}{3I_{Lf}^2}\right)I_o^2 \\ P_{RL} = R_LI_{LFrms}^2 = R_L\left(1+\dfrac{\Delta i_{Lf}^2}{3I_{Lf}^2}\right)I_{Lf}^2 \\ P_{VF} = V_FI_{Drms} = V_FI_{Lf}\sqrt{\left(1+\dfrac{\Delta i_{Lf}^2}{3I_{Lf}^2}\right)(1-D_{y)}} = V_FI_o\sqrt{\left(1+\dfrac{\Delta i_{Lf}^2}{3I_{Lf}^2}\right)\dfrac{1}{1-D_y}} \end{cases} \tag{3.30}$$

Fig. 3-7 and Fig. 3-8 are the continuous equivalent circuit diagrams of non-ideal PWM controlled source that get from Fig. 3-5, Fig. 3-6 and (3.30). These derivations of equations are based on the principle of conservation of energy, that is, the power loss of on resistances of switch Q and diode D and the loss from forward voltage drop V_F of diode D are constant in each branch.

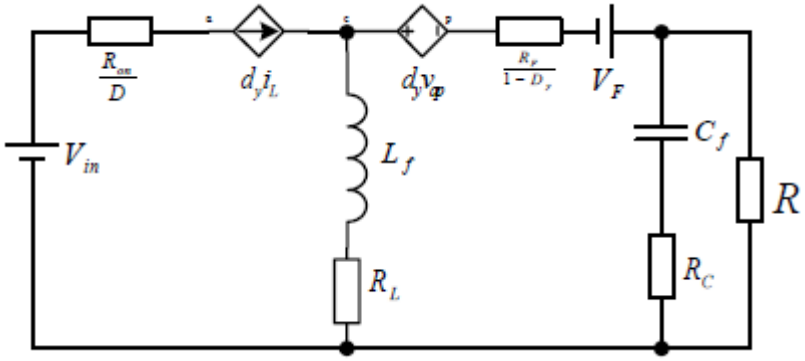

Fig. 3-7 Equivalent circuit diagram of parasitic parameters in the original branch

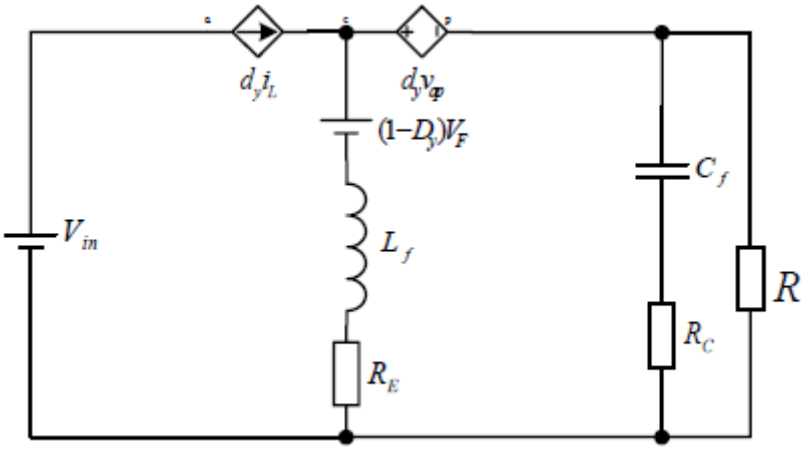

Fig. 3-8 Equivalent circuit diagram of parasitic parameters in the inductive branch

Fig. 3-7 is the equivalent diagram of parasitic parameters in the original branch. Fig. 3-8 is the equivalent diagram of parasitic parameters in the inductive branch. In Fig. 3-8, where R_E is the equivalent resistance of the inductive branch:

$$R_E = R_L + (1 + D_y)R_F + D_y R_{on} \tag{3.31}$$

Fig. 3-9 shows that the controlled source in Fig. 3-8 is replaced by ideal transformer, which is the Large-signal averaging model of continuous current mode.

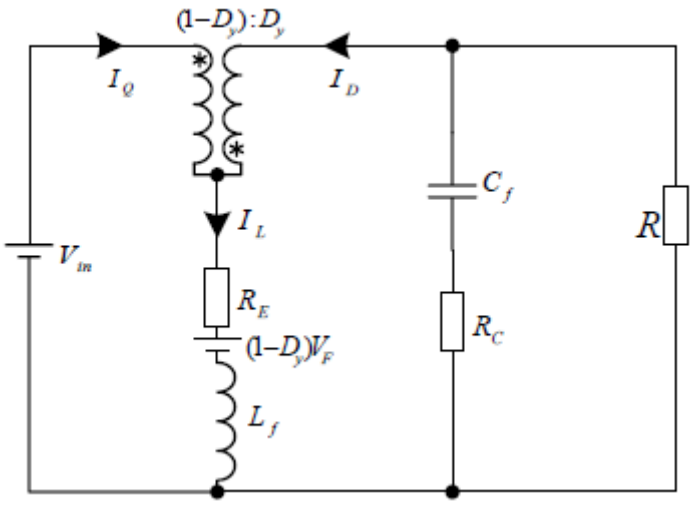

Fig. 3-9 Large-signal averaging model for continuous current mode

When the circuit is working in the steady state, the increment $\Delta i_{Lf(+)}$ of inductive current during the Q is on equals to the decrement $\Delta i_{Lf(-)}$ during the Q is off. Then:

$$D_y = \frac{V_o + V_F + I_{Lf}(R_L + R_F)}{V_{in} + V_o + V_F + I_{Lf}(R_{on} - R_F)} \tag{3.32}$$

$$V_o = \frac{D_y}{1 - D_y} V_{in} - \frac{1}{1 - D_y} I_{Lf} R_E - V_F \tag{3.33}$$

$$I_{Lf} = \frac{I_Q}{D_y} = \frac{I_D}{1 - D_y} = \frac{1}{1 - D_y} \times \frac{V_o}{R} \tag{3.34}$$

If the parasitic parameters are ignored and V_F=0, R_L=R_F=R_{on}=R_E=0, equation (3.32) and (3.33) can be simplified to equation (3.5) and (3.6). So, equation (3.5) and (3.6) are the particular case of equation (3.33).

3.3.2 DC Averaging Model

If the disturbances $\hat{v}_{in} = \hat{v}_o = \hat{\imath}_L = \hat{d}_y = 0$, the capacitor C_f is open circuit and inductor

L_f is short out, then from Fig. 3-9 and equation (3.26) and (3.27), we have Fig. 3-10 which is the DC equivalent circuit model of the continuous current mode.

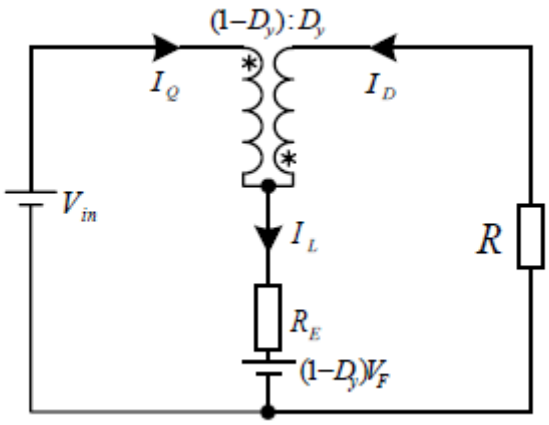

Fig. 3-10 DC averaging model for continuous current mode

The efficiency is:

$$\eta = \frac{V_o I_o}{V_{in} I_m} = \frac{V_o I_D}{V_{in} I_Q} = \frac{1}{1 + \frac{V_F}{V_o} + \frac{1}{(1-D)^2} \times \frac{R_E}{R}}$$

$$= \frac{1 - \frac{(1-D)V_F}{DV_{in}}}{1 + \frac{DR_{on} + (1-D)R_F + R_L}{(1-D)^2 R}} \tag{3.35}$$

3.3.3 Small Signal Linear Model

From equation (3.26) and (3.27), if the DC component $D_y I_L$=0 and $D_y V_{in}$=0:

$$d_y i_L = I_L \hat{d}_y + D\hat{\imath}_L \tag{3.36}$$

$$d_y v_{in} = V_{in} \hat{d}_y + D_y \hat{v}_{in} \tag{3.36}$$

From Fig. 3-9 and equation (3.36) and (3.37), we can have the small signal linear model of

continuous current mode, as shown in Fig. 3-11:

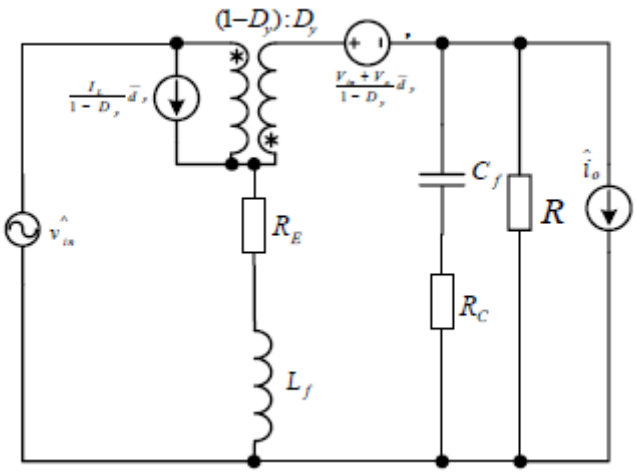

Fig. 3-11 small signal linear model of continuous current mode

From Fig. 3-13, we can have the transfer function of continuous current mode of non-ideal Buck-Boost converter.

1) The transfer function of $G_{vd}(s)$ (where $\hat{d}_y(s)$ is duty ratio and $\hat{v}_o(s)$ is output voltage)

   If $\hat{v}_{in}(s) = 0, \hat{\imath}_o(s) = 0,$ then:

$$G_{vd}(s) = \frac{\hat{v}_o(s)}{\hat{d}_y(s)}\Big|_{\hat{v}_o(s)=0,\hat{\imath}_o(s)=0} = \frac{\frac{V_{in}+V_o}{1-D_y} - (R_E + sL_f)\frac{V_o}{(1-D_y)^3 R}}{1 + \frac{(R_E+sL_f)(sC_fR_c + sC_fR + 1)}{R(1+sC_fR_c)(1-D_y)^2}}$$

$$= \frac{(1+sC_fR_C)[R(1-D_y)(V_{in}+V_o) - \frac{(R_E+sL_f)V_o}{1-D_y}]}{R_E + R(1-D_y)^2 + s\left[L_f + R_E(R_C+R)C_f + R_CR(1-D_y)^2C_f\right] + s^2(R_C+R)L_fC_f}$$

$$= G_{vd0}\frac{(1+\frac{s}{\omega_{z1}})(1-\frac{s}{\omega_{z5}})}{1+2\xi\left(\frac{s}{\omega_0}\right)+(\frac{s}{\omega_0})^2} = G_{vd0}\frac{(1+\frac{s}{\omega_{z1}})(1-\frac{s}{\omega_{z5}})}{1+\left(\frac{s}{Q\omega_0}\right)+s^2(\frac{1}{\omega_0})^2} \quad (3.38)$$

2) The transfer function $Z_o(s)$ (output impedance) (where $\hat{\imath}_o(s)$ is output current

and $\hat{v}_o(s)$ is output voltage)

If $\hat{v}_{in}(s) = 0, \hat{d}_y(s) = 0$, then:

$$Z_O(s) = \frac{\hat{v}_o(s)}{\hat{\imath}_o(s)}\Big|_{\hat{v}_o(s)=0,\hat{d}_y(s)=0} = \frac{\frac{R_E + sL_f}{(1-D_y)^2}}{1 + \frac{(R_E + sL_f)(sC_fR_c + sC_fR + 1)}{R(1 + sC_fR_c)(1-D_y)^2}}$$

$$= \frac{(1 + sC_fR_C)R(R_E + sL_f)}{R_E + R(1-D_y)^2 + s\left[L_f + R_E(R_C + R)C_f + R_CR(1-D_y)^2C_f\right] + s^2(R_C + R)L_fC_f}$$

$$= Z_{o0}\frac{\left(1 + \frac{s}{\omega_{z1}}\right)\left(1 + \frac{s}{\omega_{z2}}\right)}{1 + 2\xi\left(\frac{s}{\omega_0}\right) + \left(\frac{s}{\omega_0}\right)^2} = Z_{o0}\frac{\left(1 + \frac{s}{\omega_{z1}}\right)\left(1 + \frac{s}{\omega_{z2}}\right)}{1 + \left(\frac{s}{Q\omega_0}\right) + s^2\left(\frac{1}{\omega_0}\right)^2} \quad (3.39)$$

3) The transfer function $Y_i(s)$ (transfer admittance) (where $\hat{\imath}_L(s)$ is inductive current and $\hat{v}_{in}(s)$ is input voltage)

If $\hat{\imath}_o(s) = 0, \hat{d}_y(s) = 0$, then:

$$Y_i(s) = \frac{\hat{\imath}_L(s)}{\hat{v}_{in}(s)}\Big|_{\hat{\imath}_o(s)=0,\hat{d}_y(s)=0} = \frac{\frac{D_y}{1-D_y}}{\frac{R_E + sL_f}{1-D_y} + \frac{(1-D_y)(sC_fR_c + 1)}{1 + sC_fR_c + sC_fR}}$$

$$= \frac{D_y(1 + sC_fR_C + sC_fR)}{R_E + R(1-D_y)^2 + s\left[L_f + R_E(R_C + R)C_f + R_CR(1-D_y)^2C_f\right] + s^2(R_C + R)L_fC_f}$$

$$= Y_{i0}\frac{1 + \frac{s}{\omega_{z3}}}{1 + 2\xi\left(\frac{s}{\omega_0}\right) + \left(\frac{s}{\omega_0}\right)^2} = Y_{i0}\frac{1 + \frac{s}{\omega_{z3}}}{1 + \left(\frac{s}{Q\omega_0}\right) + s^2\left(\frac{1}{\omega_0}\right)^2} \quad (3.40)$$

4) The transfer function $A_u(s)$ (voltage transfer ratio) (where $\hat{v}_o(s)$ is output voltage and $\hat{v}_{in}(s)$ is input voltage)

If $\hat{\imath}_o(s) = 0, \hat{d}_y(s) = 0$, then:

$$A_u(s) = \frac{\hat{v}_o(s)}{\hat{v}_{in}(s)} \mid_{\hat{\imath}(s)=0,\hat{d}_y(s)=0} = \frac{\frac{D_y}{1-D_y}}{1 + \frac{(R_E + sL_f)(sC_fR_c + sC_fR + 1)}{R(1 + sC_fR_c)(1-D_y)^2}}$$

$$= \frac{RD_y(1 + sC_fR_C)(1-D_y)}{R_E + R(1-D_y)^2 + s\left[L_f + R_E(R_C + R)C_f + R_CR(1-D_y)^2C_f\right] + s^2(R_C + R)L_fC_f}$$

$$= A_{u0}\frac{1 + \frac{s}{\omega_{z1}}}{1 + 2\xi\left(\frac{s}{\omega_0}\right) + \left(\frac{s}{\omega_0}\right)^2} = A_{u0}\frac{1 + \frac{s}{\omega_{z1}}}{1 + \left(\frac{s}{Q\omega_0}\right) + s^2\left(\frac{1}{\omega_0}\right)^2} \quad (3.41)$$

5) The transfer function $A_i(s)$ (current transfer ratio) (where $\hat{\imath}_L(s)$ is inductive current and $\hat{\imath}_o(s)$ is output current)

If $\hat{v}_{in}(s) = 0, \hat{d}_y(s) = 0$, then:

$$A_i(s) = \frac{\hat{\imath}_L(s)}{\hat{\imath}_o(s)} \mid_{\hat{v}(s)=0,\hat{d}_y(s)=0} = \frac{-\frac{1}{1-D_y}}{1 + \frac{(R_E + sL_f)(sC_fR_c + sC_fR + 1)}{R(1 + sC_fR_c)(1-D_y)^2}}$$

$$= \frac{-R(1 + sC_fR_C)(1-D_y)}{R_E + R(1-D_y)^2 + s\left[L_f + R_E(R_C + R)C_f + R_CR(1-D_y)^2C_f\right] + s^2(R_C + R)L_fC_f}$$

$$= A_{i0}\frac{1 + \frac{s}{\omega_{z1}}}{1 + 2\xi\left(\frac{s}{\omega_0}\right) + \left(\frac{s}{\omega_0}\right)^2} = A_{i0}\frac{1 + \frac{s}{\omega_{z1}}}{1 + \left(\frac{s}{Q\omega_0}\right) + s^2\left(\frac{1}{\omega_0}\right)^2} \quad (3.42)$$

6) The transfer function $G_{id}(s)$ (where $\hat{\imath}_L(s)$ is inductive current and $\hat{d}_y(s)$ is duty ratio)

If $\hat{v}_{in}(s) = 0, \hat{\imath}_o(s) = 0$, then:

$$G_{id}(s)=\frac{\hat{\imath}_L(s)}{\hat{d}_y(s)}\,|_{\hat{v}(s)=0,\hat{\imath}_o(s)=0}=\frac{\dfrac{V_o}{R\left(1-D_y\right)^2}+\dfrac{(V_{in}+V_o)\left(sC_fR_c+sC_fR+1\right)}{R\left(1+sC_fR_c\right)\left(1-D_y\right)^2}}{1+\dfrac{\left(R_E+sL_f\right)\left(sC_fR_c+sC_fR+1\right)}{R\left(1+sC_fR_c\right)\left(1-D_y\right)^2}}$$

$$=\frac{V_{in}+2V_o+sC_f[V_oR_c+(V_{in}+V_o)(R_c+R)]}{R_E+R\left(1-D_y\right)^2+s\left[L_f+R_E(R_C+R)C_f+R_CR\left(1-D_y\right)^2C_f\right]+s^2(R_C+R)L_fC_f}$$

$$=G_{id0}\frac{1+\dfrac{s}{\omega_{z4}}}{1+2\xi\left(\dfrac{s}{\omega_0}\right)+\left(\dfrac{s}{\omega_0}\right)^2}=G_{id0}\frac{1+\dfrac{s}{\omega_{z4}}}{1+\left(\dfrac{s}{Q\omega_0}\right)+s^2\left(\dfrac{1}{\omega_0}\right)^2} \tag{3.43}$$

$$Where\begin{cases} G_{vd0}=\dfrac{R\left(1-D_y\right)(V_{in}+V_o)-\dfrac{R_EV_o}{1-D_y}}{R_E+R\left(1-D_y\right)^2} \\ Z_{o0}=\dfrac{RR_E}{R_E+R\left(1-D_y\right)^2} \\ Y_{i0}=\dfrac{D_y}{R_E+R\left(1-D_y\right)^2} \\ A_{u0}=\dfrac{RD_y\left(1-D_y\right)}{R_E+R\left(1-D_y\right)^2} \\ A_{i0}=\dfrac{-R\left(1-D_y\right)}{R_E+R\left(1-D_y\right)^2} \\ G_{id0}=\dfrac{V_{in}+2V_O}{R_E+R\left(1-D_y\right)^2} \end{cases} \tag{3.44}$$

$$
\begin{cases}
Corner\ frequency\ \omega_0 = \sqrt{\dfrac{R_E + R\left(1 - D_y\right)}{(R_C + R)L_f C_f}} \\
Damping\ ratio\ \xi = \dfrac{R_E R C_f + R_C R C_f \left(1 - D_y\right)^2 + R_E R_C C_f + L_f}{2\sqrt{\left[R_E + R\left(1 - D_y\right)^2\right](R_C + R)L_f C_f}} \\
Quality\ factor\ Q = \dfrac{1}{2\xi} \\
Left\ half\ plane\ zero\ \omega_{z1} = \dfrac{1}{R_C C_f} \\
\omega_{z2} = \dfrac{R_E}{L_f} \\
\omega_{z3} = \dfrac{1}{(R_E + R)C_f} \\
\omega_{z4} = \dfrac{C_f[V_o R_C + (V_{in} + V_o)(R_C + R)}{V_{in} + 2V_o} \\
Right\ half\ plane\ zero\ \omega_{z5} = \dfrac{R\left(1 - D_y\right)^2 - R_E}{L_f} + \dfrac{R\left(1 - D_y\right)^2}{L_f} \cdot \dfrac{V_{in}}{V_o}
\end{cases}
\tag{3.45}
$$

3.4 Summary

This chapter analyzes the rationale of buck-boost converter, get the equations of current effective value and turn-off voltage of the MOSFET, and the current mean value, reverse voltage, inductance and capacitance of the diode. Also, the parameters has been calculated.

In addition, Large-signal averaging model, DC averaging model and small signal linear model of the non-ideal Buck-Boost converter for continuous mode has been analyzed, the transfer function has been derived. This modeling approach has the clear physical meaning and practical value, and is conducive to the further analysis and design of control circuit.

CHAPTER 4 DEVELOPMENT AND CONTROL STRATEGY OF DC-DC CONVERTER

4.1 Controller Design

A SISO switching fuzzy proportional-integral controller is designed for output voltage regulation. The error between the set point and converter output forms input to the controller while the output from the controller is translated to a variable duty cycle signal which drives the power MOSFET. The control law can be described as:

$$u_c(t) = sat\left(u_{FLC}\big(e(t)\big) + K_I \int_0^t e(t)\, d_t \right) \tag{4.1}$$

Where, $u_{FLC}(e(t))$ is the fuzzy proportional controller, defined as:

$$u_{FLC}\big(e(t)\big) = \begin{cases} u_{RFC}\big(e(t)\big), e(t) \geq 0 \\ u_{LFC}\big(e(t)\big), e(t) < 0 \end{cases} \tag{4.2}$$

The controller structure is shown in Fig. 4-1. This section describes the stages in the design of fuzzy logic controller.

4.1.1 Fuzzification

The error signal corresponding to the positive section of universe of discourse i.e., e ϵ [0,3], is described by seven fuzzy sets namely Zero-Right (ZR), Positive Small (PS), Positive Medium (PM), Positive Large (PL), Positive Big (PB), Positive too Big (PTB) and Positive-Cover (PC). These fuzzy sets form 'Right Fuzzy Controller (RFC)' and employ

triangular membership functions with the exception of set 'PTB' which is described by trapezoidal membership function as shown in Fig. 4-2. The degree of belongingness of the linguistic variable 'error' to these fuzzy sets is computed based on the following expressions:

$$\mu_{ZR}(e) = \begin{cases} -3.3e + 1, & 0 \le e \le 0.3 \\ 0, & 0.3 \le e, e \le 0 \end{cases} \tag{4.3}$$

$$\mu_{PS}(e) = \begin{cases} 3.3e, & 0 \le e \le 0.3 \\ -3.3e + 2, & 0.3 \le e, e \le 0 \end{cases} \tag{4.4}$$

$$\mu_{PM}(e) = \begin{cases} -3.3e - 1, & 0.3 \le e \le 0.6 \\ -3.3e + 3, & 0.6 \le e \le 0.9 \end{cases} \tag{4.5}$$

$$\mu_{PL}(e) = \begin{cases} 3.3e - 2, & 0.6 \le e \le 0.9 \\ -3.3e + 4, & 0.9 \le e \le 1.2 \end{cases} \tag{4.6}$$

$$\mu_{PB}(e) = \begin{cases} 3.3e - 3, & 0.9 \le e \le 1.2 \\ -3.3e + 5, & 1.2 \le e \le 1.5 \end{cases} \tag{4.7}$$

$$\mu_{PTB}(e) = \begin{cases} 3.3e - 4, & 1.2 \le e \le 1.5 \\ 1, & e \ge 1.5 \end{cases} \tag{4.8}$$

$$\mu_{PC}(e) = \begin{cases} -0.67e + 1, & 0 \le e \le 1.5 \\ 0, & e \ge 1.5 \end{cases} \tag{4.9}$$

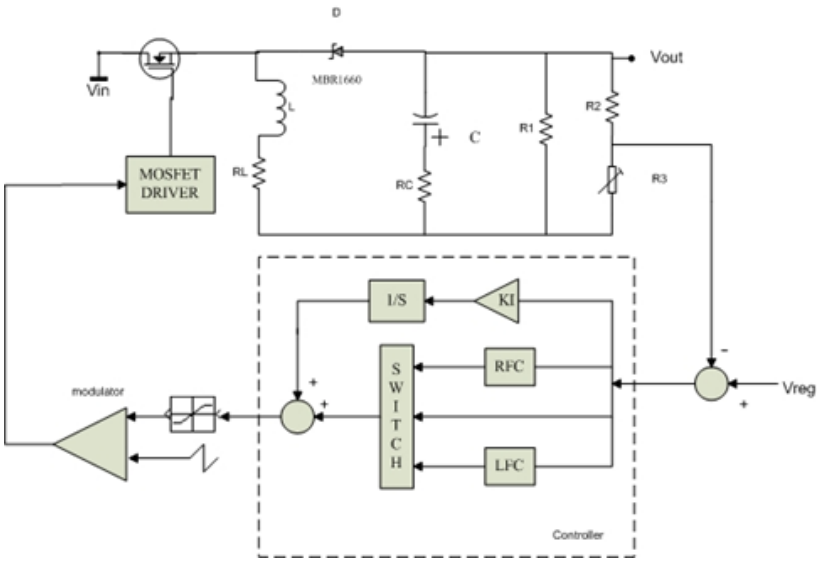

Fig. 4-1 Block diagram for controller section

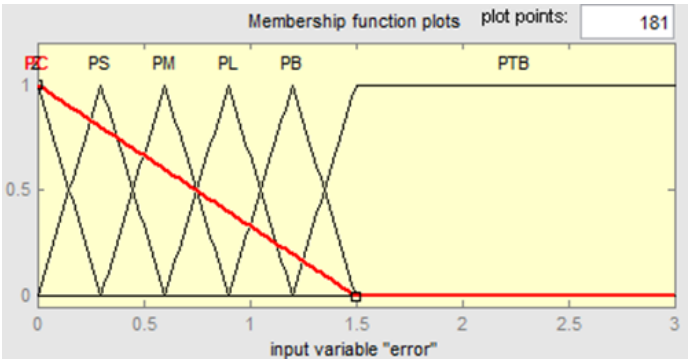

Fig. 4-2 Fuzzy sets for RFC

The output from RFC is described by six singletons namely ER, R1, R2, R3, R4, and R5. The location of singletons depicts the variation in reference voltage which is used by the modulator to generate variable duty cycle waveform for controlling the converter. The assigned values are shown in Table 4-1.

Table 4-1 Singletons for RFC

Singleton	Location of Singleton
ER	0.10
R1	0.15
R2	0.20
R3	0.25
R4	0.30
R5	0.35

Similar to RFC, we define the 'Left Fuzzy Controller (LFC)' corresponding to the negative portion of the universe of discourse i.e., e ϵ [-3,0]. LFC also utilizes seven fuzzy sets for describing the behavior of the converter. Thee fuzzy sets include Zero-Left (ZL), Negative Small (NS), Negative Medium (NM), Negative Large (NL), Negative Big (NB), and Negative-Cover (NC). Again, all these sets use triangular membership function except 'NB' which uses trapezoidal membership function. The fuzzy sets for LFC are shown in Fig. 4-3. The degree of membership of 'error' to these sets is found using a set of expressions which can be derived in a similar fashion as were obtained for RFC. The output from LFC is also described by a set of singletons namely El, L1, L2, L3, L4, and L5. The location of these singletons is listed in Table 4-2.

4.1.2 Fuzzy Rule Base

The rule bases of both 'RFC' and 'LFC' controllers contain seven rules. These rules map

the error signal between the set point and converter output to a variable control voltage used for the generation of pulse width modulated signal to drive the MOSFET. These rule bases are constructed through virtual experimentation in MATLAB environment and are shown in Table 4-3 and 4-4. The control surfaces for 'RFC' and 'LFC' are shown in Fig. 4-4 and 4-5 respectively. It should be noted that non-linearity in the surfaces is introduced through the inclusion of cover membership functions.

Table 4-2 Singletons for LFC

Singleton	**Location of Singleton**
EL	0.10
L1	0.08
L2	0.06
L3	0.04
L4	0.02
L5	0.00

4.1.3 Defuzzification

The defuzzification process generates the crisp value from the fuzzy value. The weighted average method is used as a defuzzification strategy in the present work which can be described as:

$$u_{RFC}\big(e(t)\big) = \sum_{i-1}^{7} w_i\big(e(t)\big)s_{t,i} \,/\, \sum_{i-1}^{7} w_i\big(e(t)\big) \tag{4.10}$$

Where, $w_i(e(t))$ is the firing strength of the 'i^{th}' rule and $s_{t,i}$ is the singleton defined for the 'i^{th}' rule. A similar expression can be written for LFC.

Table 4-3 Rule base for RFC

Rule No.	Rule Definition
01	IF e is ZR THEN u is ER
02	IF e is PS THEN u is R1
03	IF e is PM THEN u is R2
04	IF e is PL THEN u is R3
05	IF e is PB THEN u is R4
06	IF e is PTB THEN u is R5
07	IF e is PC THEN u is ER

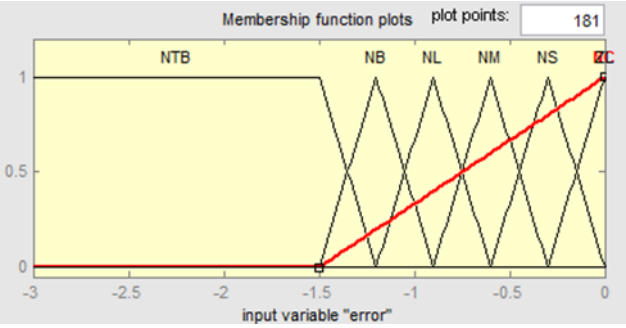

Fig. 4-3 Fuzzy sets for LFC

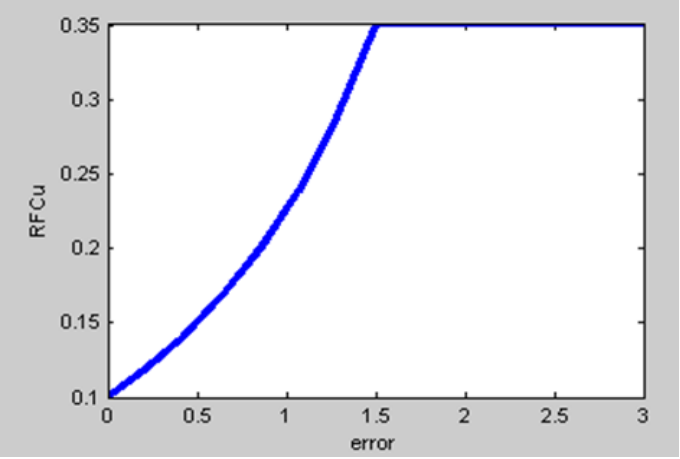

Fig. 4-4 Control surface for RFC

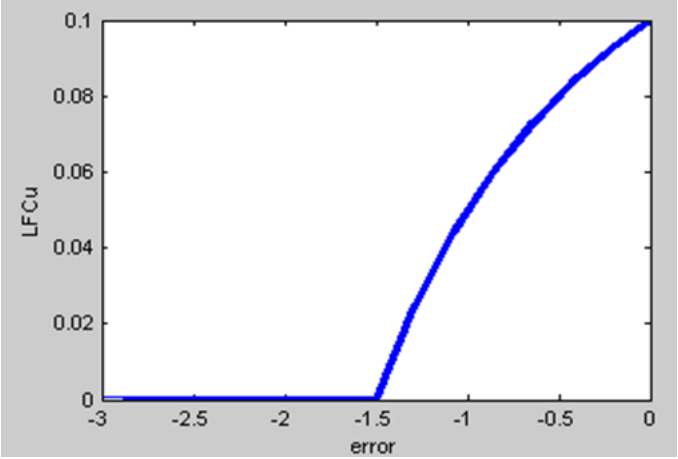

Fig. 4-5 Control surface for LFC

Table 4-4 Rule base for LFC

Rule No.	Rule Definition
01	IF e is ZL THEN u is EL
02	IF e is NS THEN u is L1
03	IF e is NM THEN u is L2
04	IF e is NL THEN u is L3
05	IF e is NB THEN u is L4
06	IF e is NTB THEN u is L5
07	IF e is NC THEN u is EL

4.2 Simulation Results

The proposed controller is simulated in MATLAB/Simulink environment for different values of the line voltages to mimic the variable voltage from the permanent-magnet linear generator. A PI controller is also designed for the purpose of comparison. The integral constants for the both the controllers is the same while the proportional constant in PI

controller represents the singleton corresponding to 'Exact (E)' membership function of the fuzzy logic controllers. It will be shown that the proportional constant of PI controller, once set to different singletons, produces erratic results.

The response of the controllers for regulating the output voltage corresponding to input voltage, Vin=2V, is shown in Fig. 4-6. It can be seen that FLC has better rise time as compared to PI controller. However, both the controllers exhibited the same settling time. The overshoot is avoided in the response of the controllers by adjusting the integral gain and it is set at, KI=1.5.

Figures 4-7 and 4-8 shows the degradation in the performance of the PI controller when the proportional gain is set around the singletons 'R2' and 'R4' respectively. Thus it can be concluded that it is not mere using high gains with FLC which improves the converter transient performance.

The response of controllers for the line voltages, V_{in}=1.5V and V_{in}=2.5V is shown in Figs. 4-9 and 4-10 respectively. Reference tracking by the controller for V_{in}=2.0V is shown in Fig. 4-11.

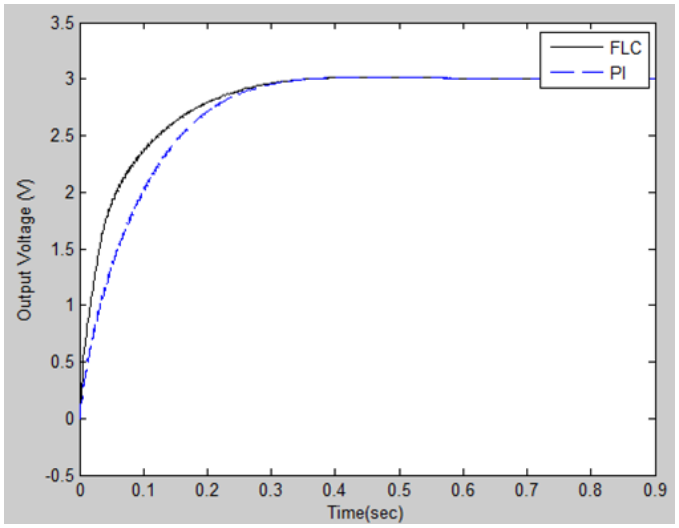

Fig. 4-6 Voltage regulation (V_{in}=2V)

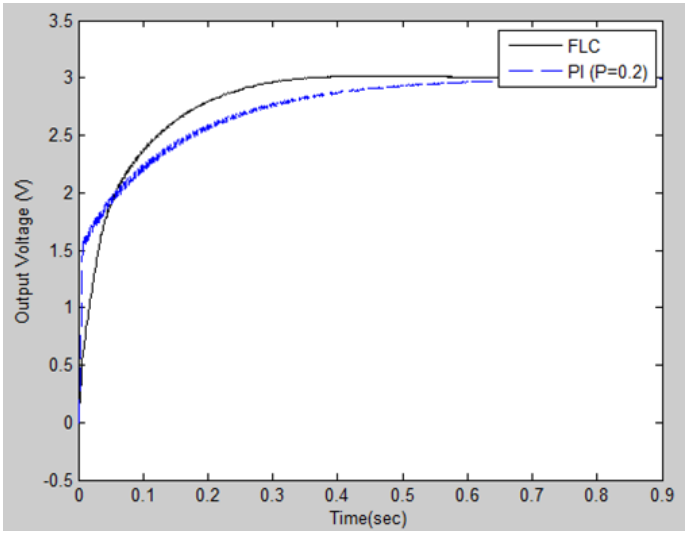

Fig. 4-7 Voltage regulation (V_{in}=2V)

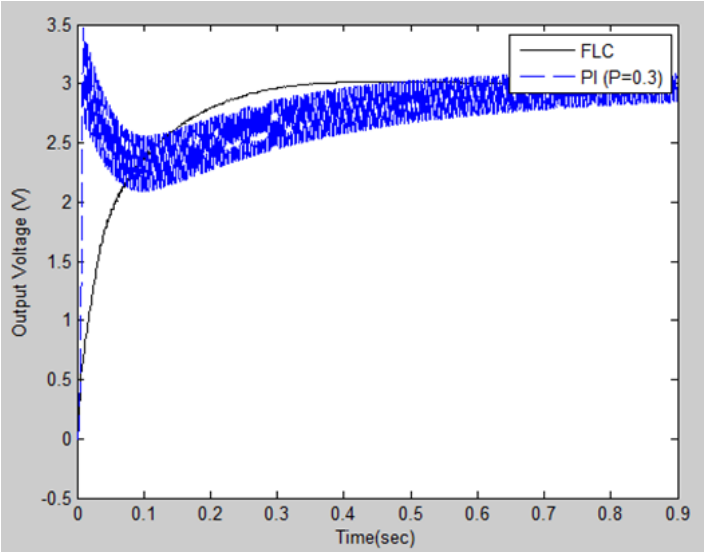

Fig. 4-8 Voltage regulation (V_{in}=2V)

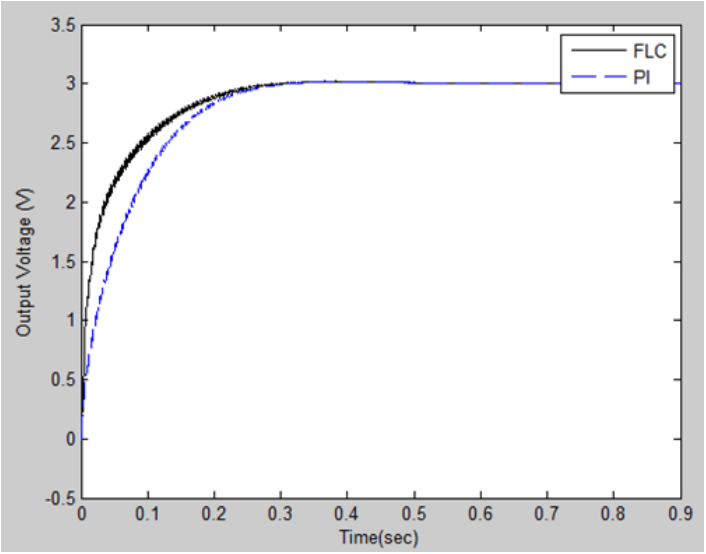

Fig. 4-9 Voltage regulation (V_{in}=2.5V)

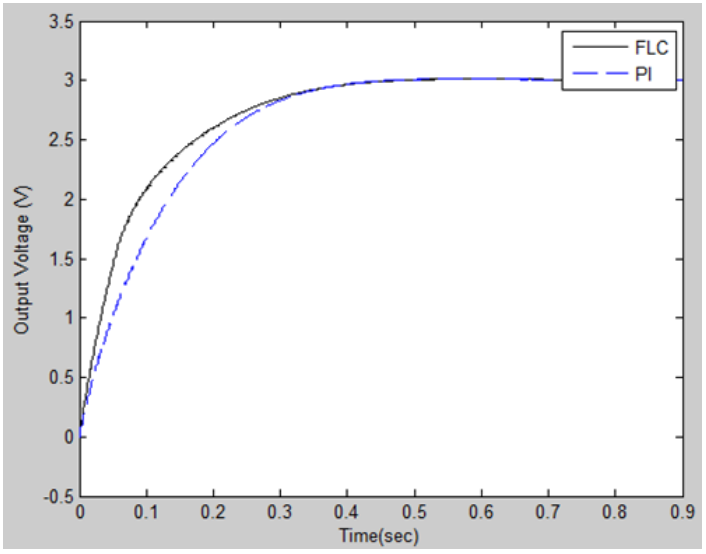

Fig. 4-10 Voltage regulation (V_{in}=1.5V)

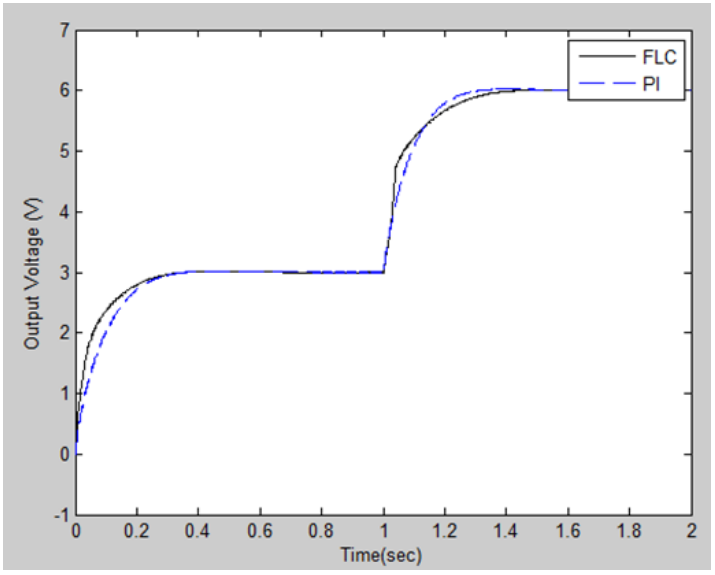

Fig. 4-11 Reference tracking (V_{in}=2.0V)

CHAPTER 5 EXPERIMENT OF VIBRATION ENERGY HARVESTING DEVICE FOR VEHICLE SUSPENSION SYSTEM

5.1 Experiment System Constitution

The experiment system can be divided into three parts, which are the permanent magnet linear generator, the associated hardware and the vibration simulation model.

5.1.1 Permanent Magnet Linear Generator

The design of the permanent magnet linear generator has been described in Chapter 2. The slotted generator design was difficult to make due to the cylindrical shape of the device. It was proposed that the cylinder be segmented alternatively between slots and spaces. This would give easy access to the inside so that the rest of the generator can be assembled. An apparatus was constructed (Fig. 5-1) as a form so that the windings could be wound to accurate dimensions. Exiting wires will run up the through holes drilled in the end cap and up through the top. Two end caps should be used, but one at this time will suffice, due to cost and time constraints.

Fig. 5-1 Winding apparatus

The tool shown in Fig. 5-1 was made to make it easier to make each winding. The slot in the middle has the same dimensions as a slot in the generator this provides something to get the correct inner diameter of the winding while maintaining the proper thickness. The tool comes apart once a winding has been made and the winding slides off the center piece.

The generator will consist of a stack of steel parts held together by long threaded rods that run the length of the body. This is what gives the generator the shape of a shock absorber while holding it together.

As the stack was built up a connection between each winding was soldered. In total there were 20 connections along the length of the generator. This actually cause many problems when making the device because of broken or loose windings or connections shorting out to the steel body of the generator and there by shorting the most windings. Due to this problem extra insulation was added to each winding and also each connection. This fixed

the shorting problem however the extra insulation reduced the air gap too much. This is the current problem, the forcer can still move through the body but it has significant friction. The assembled generator is shown in Fig. 5-2.

Fig. 5-2 Assembled generator

5.1.2 The Associated Hardware

The hardware section is meant to convert the variable voltage from the generator to a desired fixed voltage. It can be divided into various sub-units and the interconnection between these units is depicted in Fig. 5-3 while experimental setup is shown in Fig. 5-4.

1) Bridge Rectifier: The fluctating ac voltage from the permanent magnet linear generator is converted into variable dc voltage through the use of a full bridge rectifier. The

bridge rectifier uses 1N5819 fast recovery diodes for its construction.

2) Buck-Boost Converter: The output from the bridge rectifier is regulated to a desired fixed dc voltage using a buc-boost converter. The converter consists of IRFZ44N MOSFET, IN5819 diodes, a set of inductors (750μH, 330 μH) and a set of capaciotrs (0.1μF, 4700μF, 1000μF).

3) DSP: A TMS320F2812 digital signal processor is used to generate the gate signal for MOSFET in buck-boost converter unit. The variable duty cycle signal is buffered using a gate circuitary and is fed to the MOSFET through an HCPL 3140 opto-isolator. The opto-isolator prevents the surges appearing on the dc bus which feeds the processor. The load voltage is scaled down to lie within the operating voltage limits of the processor through a voltage divider network. This lowered voltage is sensed through an analog-to-digital converter onboard the processor which runs the controller to operate the buck-boost converter.

4) Auxiliary Unit: This unit is responsible for safe operation of the hardware section by limiting the voltages to various integrated circuit chips.

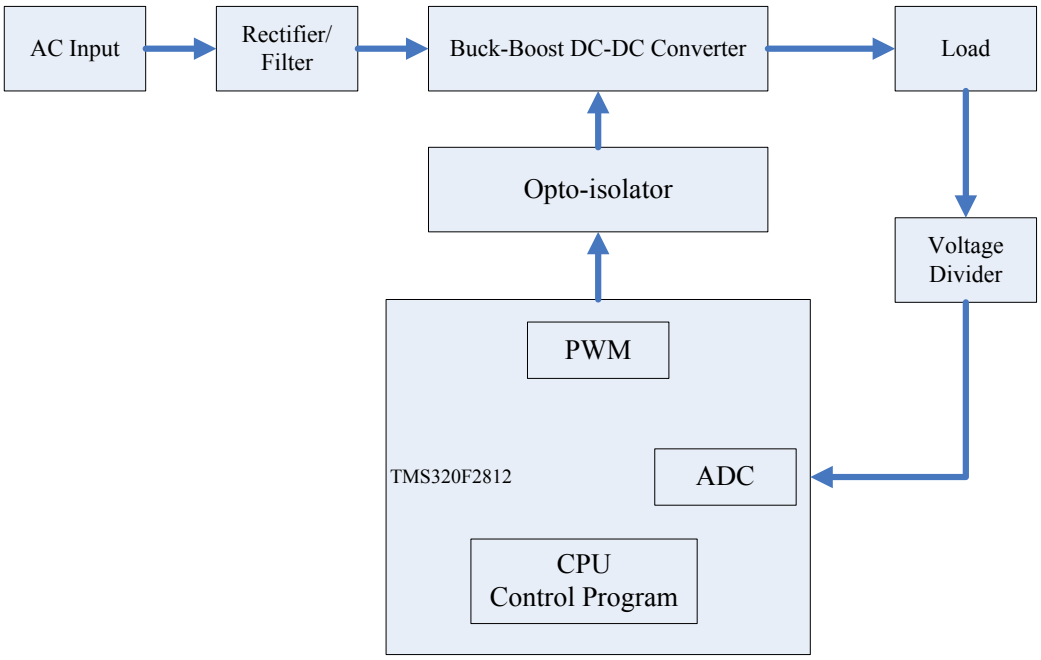

Fig. 5-3 Block diagram for hardware section

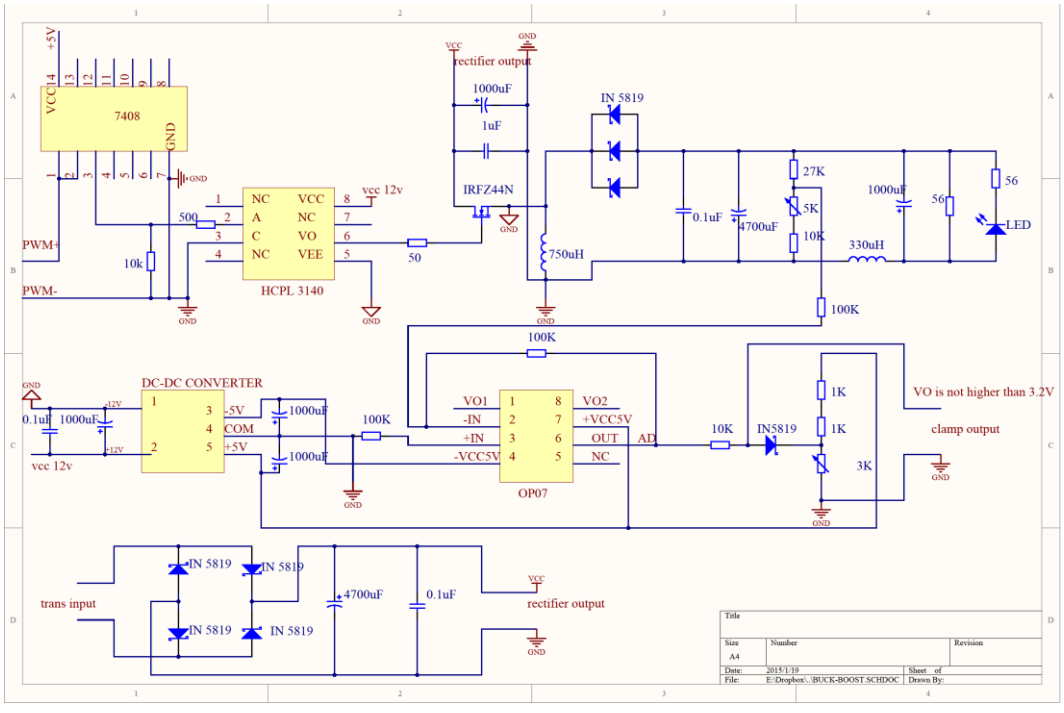

Fig. 5-4 The experiment circuit diagram

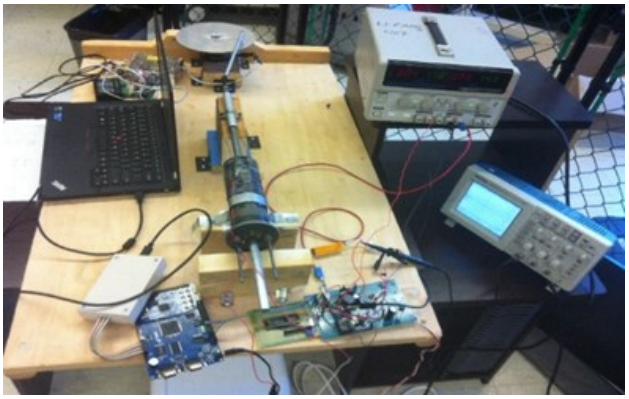

Fig. 5-5 Experimental setup

5.1.3 The Vibration Simulation Model

Vibration simulation model is simulated the vertical direction vibration process of the automobile shock absorber when vehicle is moving. In this system, a stepping motor is controlled by a microcontroller. A disk is fixed on the rotation axis of the stepping motor, and connected with a metal pole, to achieve the conversion from rotary motion to linear motion, shown in Fig. 5-6.

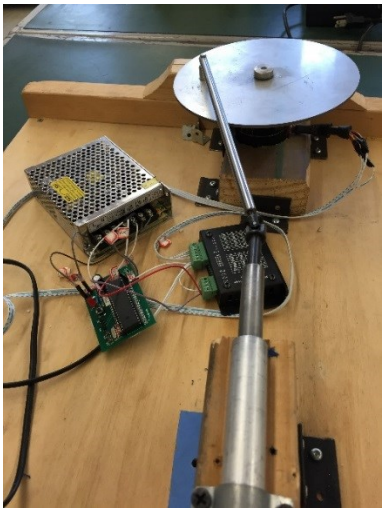

Fig. 5-6 Vibration simulation model

Rotary control system includes three modules: control module, drive module and stepper motor module. Control module uses AT89C52 single-chip microcomputer (SCM) as the controller; the drive motor uses TB6560 chip; and the stepping motor is two-phase reaction stepping motor. The system principle diagram is shown in Fig. 5-7.

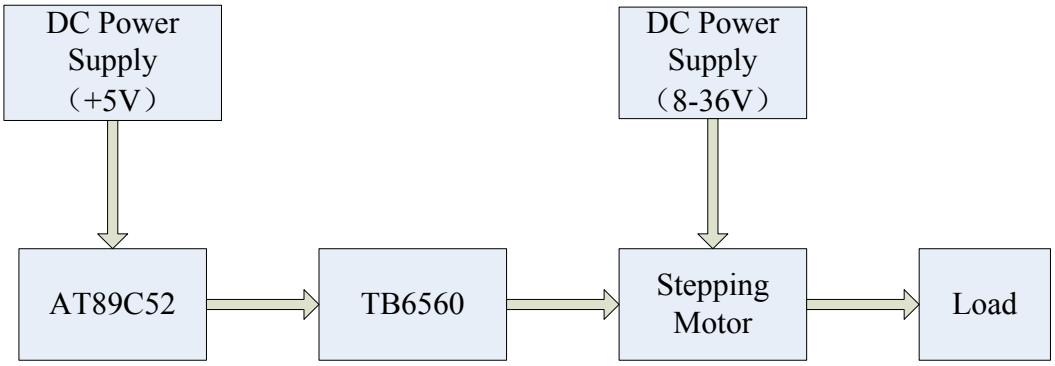

Fig. 5-7 Simulation system principle diagram

TB6560 chip has high stability and good anti-interference, can drive a variety of two-phase stepping motor, the maximum subdivision is 16, and has low voltage shut down, overcurrent protection, overheating shut down.

The output ports P1.0, P1.1 and P1.2 of AT89C52 SCM connect CK, EN and CW of TB6560 chip, to control the rotation angular frequency, start-stop and rotation direction. The control circuit diagram is shown in Fig. 5-8.

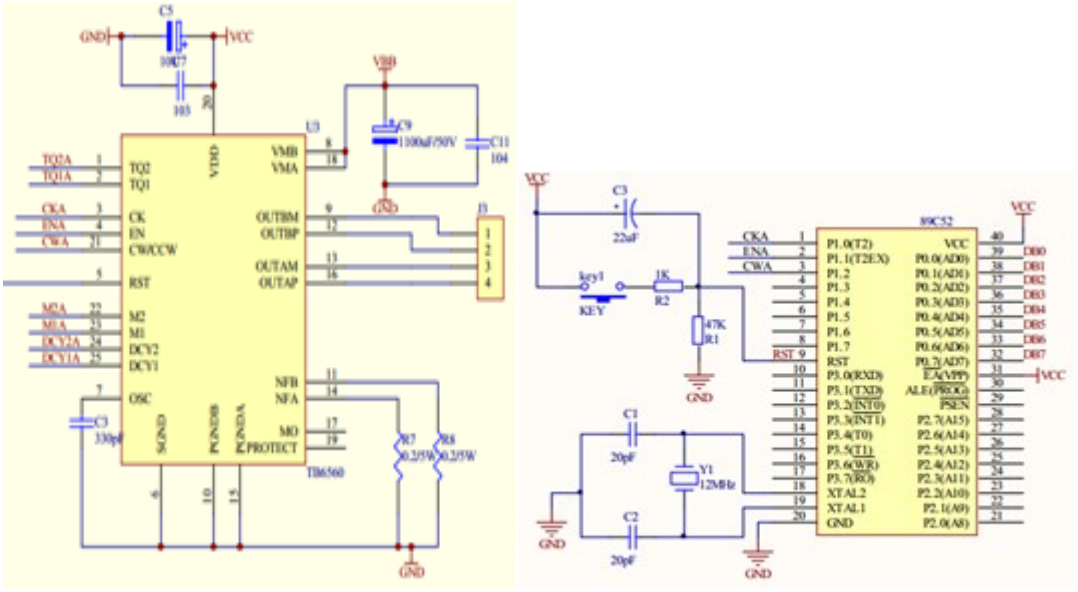

Fig. 5-8 Control circuit diagram

From some research [30], when the vehicle is moving on the road, the vertical direction vibration frequency of the shock absorber is generally less than 10 Hz, vibration amplitude is 5-20 mm. The pulse output control frequency is set as 150000 Hz, after 4-16 subdivision through TB6560 chip, the frequency of the motor can be less than 10 Hz. The flow chat of the control system is shown in Fig. 5-9.

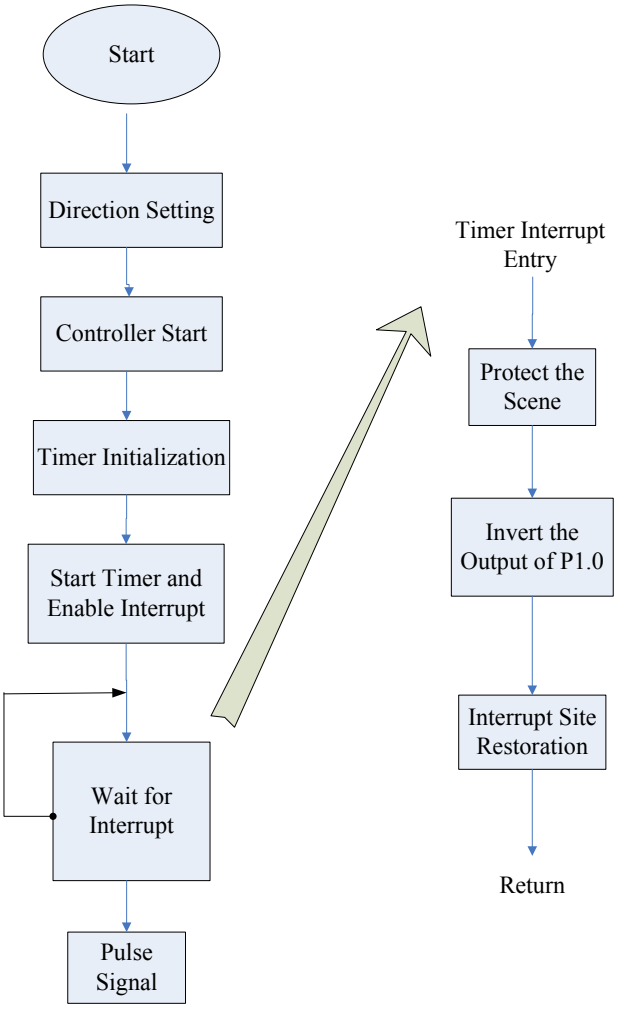

Fig. 5-9 flow chat of the control system

5.2 Experiment results

The load voltage, sampled from analog-to-digital converter (ADC) onboard the TMS320F2812 kit, is logged in MATLAB environment via UART1 channel of the digital signal processor at a baud rate of 9600bps. Fig. 5-10 shows the real time results obtained with the two controllers while regulating the load voltage to 3.0V when an input voltage of 2.0V is available from the generator. It can be seen that transient response of FLC is better

than PI controller. The zoomed portion in Fig. 5-10 shows the oscillations induced by the controllers near the set point. The lower peak in the oscillations attained by FLC shows its better performance over PI controller. The set point is changed to 5.0V while keeping the generator output at around 2.0V and the voltage regulation by the controllers is depicted in Fig. 5-11. The performance of FLC is clearly better than PI controller during transient as well as steady state.

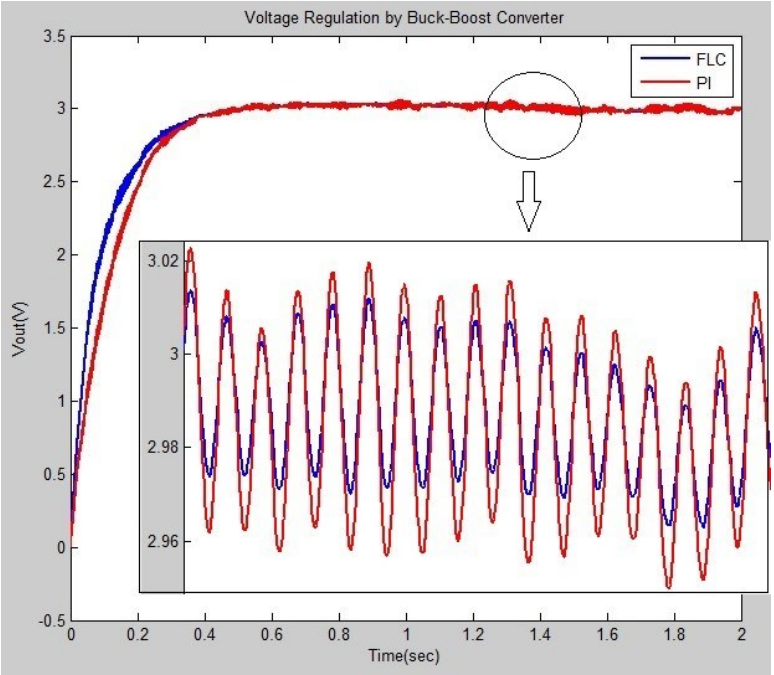

Fig. 5-10 Voltage regulation (V_{in}=2.0V)

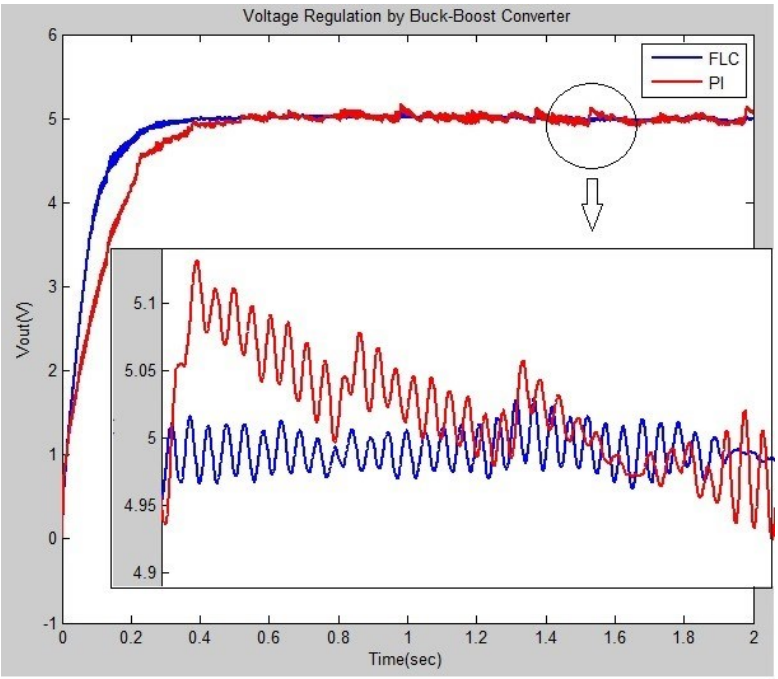

Fig. 5-11 Voltage regulation (V_{in}=2.0V)

CHAPTER 6 CONCLUSION

6.1 Summary

This thesis mainly studied on the automobile vibration energy generation and low power converter, developed and tested an automobile vibration energy generation system [31].

Vehicle vibration energy can be collected from the general suspension system with energy conversion device, with the space constraints, the electromechanical conversion device cannot be too large. Through analyzing various commonly used transfer device for vibration energy, we adopt permanent-magnet linear reciprocating generator as the transfer device. The purpose of development of automotive vibration generation system is to provide the energy supplements to the vehicle, due to the output of vibration generator is small and unstable, the DC-DC converter with stable output is studied. The main conclusions are as following:

1) Based on Faraday's law of electromagnetic induction, the theory of the permanent magnet generator used in structure design is studied. Using Faraday's law, equations of output voltage and Maxwell software simulated the magnetic flux intensity of the stators and its distribution of the components to get the magnetic flux intensity and transient voltage output. we adopt permanent-magnet linear reciprocating generator as the transfer device and produce a prototype of coreless

cylindrical linear reciprocating generator. Compared with other vibration generator, the generator has simple structure, moving light quality, so the vibration frequency can be higher, also, has a wider range of application and good for further development.

2) Based on the analysis of the rationale of the DC-DC converter, combining with the characteristics of automobile vibration energy conversion, a customized DC-DC converter is designed. This thesis designs a DSP-based control system for electrical energy transformation in which Buck-Boost converter is chosen as a control object. Besides, we construct a compound controller by combining the conventional PI control strategy with novel fuzzy control strategy. Finally, the validity of our control strategy has been verified by simulation results of the compound controller's static and dynamic performance.

3) This thesis constructs an experiment system which consists of permanent-magnet linear generator, DSP, Energy Management System. Based on the fuzzy PI control algorithm, the output voltage reaches 3.0V stably when the vibration frequency and load resistance are 10HZ and 20Ω, respectively. Experiment results have verified the practicability of our power generation system's design scheme using automobile vibration and the validity of fuzzy PI control algorithm the power management system used.

6.2 Future Work

Due to the research of the permanent magnet linear vibration generator only began in a few years, there is quite lack of study on the structure of permanent magnet linear generator. Therefore, it still need the further study on the vibration energy generation system to improve the efficiency. In the experimental device, because of the prototype of the permanent magnet linear generator was assembled manually, there is some gap between the magnet and coil, has the magnetic flux leakage and the coil windings are uneven. These are all damage the power generation efficiency. In addition, the parameters of the stators and coils of the permanent magnet linear generator still need to improve.

Due to the power of the automobile vibration generation system is low and unstable, and there has peak pulse interference in the output of the power MOSFET of the Boost-Buck converter controlled by PWM, it still need further study on the design of the capacitance and inductance, and the control strategy, to improve the stability of the output.

BIBLIOGRAPHY

[1] Shunsuke Ohashi,Tatsuro Matsuzuka. Basic characteristics of the linear synchronous generator using mechanical vibration [J]. IEEE Transactions on Magnetics, 2005, v 41, n 10, p 3829-3831.

[2] Y. Ye. Principle and application of linear motor［M］. Beijing: mechanical industry press, 2000.

[3] T.W. Thorpe, M.J, Picken. Wave energy devices and the marine environment [J]. IEE Proceedings A, 1993, v 140, n 1, p 63-70.

[4] L. Ran, M.A. Mueller, C. Ng, et al. Power conversion and control for a linear direct drive permanent magnet generator for wave energy[J]. IET Renewable Power Generation,2011,v 5, n 1, p 1–9.

[5] S. Tyrberg, R. Waters, M. Leijon. Wave Power Absorption as a Function of Water Level and Wave Height: Theory and Experiment [J]. IEEE Journal of Oceanic Engineering,2010, v 53, n 3, p 558-564.

[6] A. Wolfbrandt. Automated design of a linear generator for wave energy converters—a simplified model[J]. IEEE Trans. on Magnetics, 2006, v 42, n 7, p 1812-1819.

[7] J. Wang, D. Howe, G.W. Jewell. Fringing in tubular permanent-magnet machines: Part I. Magnetic field distribution, flux linkage and thrust force[J]. IEEE Trans. on Magnetics, 2003, v 39, n 6, p 3507-3516.

[8] J. Wang, D. Howe, G.W. Jewell. Fringing in tubular permanent-magnet machines: Part II. Cogging force and its minimization[J]. IEEE Trans. on Magnetics, 2003, v 39, n 6, p 3517-3522.

[9] C. Liu, C. Lin, C. Hwang, et al. Compact model of a slotless tubular linear generator for renewable energy performance assessments[J]. IEEE Trans. on Magnetics, 2010, v 46, n 6, p 1467-1470.

[10] K.J. Meessen, B.L.J. Gysen, J.J.H. Paulides, et al. Halbach permanent magnet shape selection for slotless tubular actuators[J]. IEEE Trans. on Magnetics, 2008, v 44, n 11, p 4305-4308.

[11] H. Polinder, M.E.C. Damen, F. Gardner,et al. Linear PM generator system for wave energy conversion in the AWS[J]. IEEE Trans. On Energy Conversion, 2004, v 19, n 3, p 583-589.

[12] H. Polinder, M.E.C. Damen, F. Gardner, et al. Design,modeling and test results of the AWS PM linear generator[J]. European Trans. on Electrical Power, 2005(15) : 245-256.

[13] D. Elwood, S.C. Yim, J, Prudell, et al. Design, construction, and ocean testing of a taut-moored dual-body wave energy converter with a linear generator power take-off [J]. Renewable Energy,2010, v 35, n 2, p 348-354.

[14] J. Prudell, M. Stoddard, E. Amon． A permanent-magnet tubular linear generator for ocean wave energy conversion [J]. IEEE Trans. on Industry Application, 2010, v 46, n 6, p 2392-2400.
[15] K. Thorburn, M. Leijon. Farm size comparison with analytical model of linear generator wave energy converters [J]. Ocean Engineering, 2007, v 34, n 5-6, p 908-916.
[16] R. Waters, M. Rahm, M. Eriksson, et al. Ocean wave energy absorption in response to wave period and amplitude offshore experiments on a wave energy converter[J]. IET Renewable Power Generation, 2011, v 5, n 11, p 465-469.
[17] C. Liu, H. Yu, M. Hu, et a1. Application of Permanent Magnet Tubular Linear Generators Using Direct-driver Wave Power Generation Take-off Systems [J]. Proceedings of the Chinese Society for Electrical Engineering, 2013, v 33,n 21, p 90-98.
[18] J. Zhang, X. Liu, Q. Chen, et a1. Design and Dynamic Analysis of Tubular Halbach PM Single Phase Linear Generator [J]. Chinese Small & Special Electrical Machines, 2014, v 42, n 8, p 20-23.
[19] P. Liu, Y. Wan, P. Li, et a1. Study on the Power Management Circuit of a Magneto electric Self-Powered Wireless Sensor [J]. Chinese Journal of Sensors and Actuators, 2008, v 21, n 8, p 297-298.
[20] C. Zhang , J. Wang , S. Li. Robust control for PWM-based DC-DC buck power converters with uncertainty via sampled-data output feedback [J/OL]. IEEE Transactions on Power Electronics, 2015, v 30, n 1, p 504-515.
[21] J.C. Rosas-Caro, J.C. Mayo-Maldonado, A. Valderrabano-Gonzalez. DC-DC multiplier boost converter with resonant switching [J/OL]. Electric Power Systems Research, 2015, v 119, p 83-90.
[22] Y. Wang , D. Yu , Y. Kim . Robust time-delay control for the DC-DC boost converter. IEEE Transactions on Industrial Electronics [J], 2014, v 61, n 9, p 4829-4837.
[23] Z. Yang , Y. Ye , Q. Lu . Design of self-tuning fuzzy PID controller on PWM DC-DC converter [J]. Lecture Notes in Electrical Engineering, 2014, v 238 LNEE, p 685-691.
[24] J. Fan, X. Zhou, L. Yang. A low power high noise immunity boost DC-DC converter using the differential difference amplifiers[C]. Proceedings of the 2009 ACM/IEEE International Symposium on Low Power Electronics and Design, 2009, p 63-68.
[25] A. Salah-Eddine, D. Nicolas, H. Walid. Ultra-low power, low voltage, self-powered resonant DC-DC converter for energy harvesting. Journal of Low Power Electronics, 2013, v 9, n 1, p 103-117.
[26] D. Nicolas, A. Bruno, B. François. A 140 mV self-starting 10 mW DC/DC converter for powering low-power electronic devices from low-voltage microbial fuel cells [J]. Journal of Low Power Electronics, 2012, v 8, n 4, p 485-497.
[27] W. Choi. High-efficiency DC-DC converter with fast dynamic response for low-voltage photovoltaic sources [J]. IEEE Transactions on Power Electronics, 2013, v 28, n 2, p 706-716.

[28] M.K. Kazimierczuk. (2008) Buck-Boost PWM DC-DC Converter, in Pulse-Width Modulated DC-DC Power Converters, John Wiley & Sons, Ltd., Chichester, West Sussex. doi: 10.1002/9780470694640.ch4

[29] C. Ouyang. Study and Modeling Analysis on DC-DC Switching Converter [D]. Nanjing University of Aeronautics and Astronautics, 2004.

[30] X. Tang, T. Lin, and L. Zuo. Design and Optimization of a Tubular Linear Electromagnetic Vibration Energy Harvester [J]. IEEE/ASME Transactions on Mechatronics, 2014, v 19, n 2.

[31] Y. Pu, J. Gu, U. Farooq and Y. Xu. Fuzzy Logic Based Control of Vibration Energy Harvesting Device for Automotive Suspension System [C]. IEEE International Conference on Information and Automation, 2014, p 592-597.